Determinants of Astrocytic Pathology in Stem Cell Models of Primary Tauopathies

Kimberly L. Fiock PhD[1,2], Jordan Hook BS[1,4], Marco M. Hefti MD*[1,2,3]

[1]Department of Pathology, University of Iowa, Iowa City, IA

[2]Experimental Pathology Graduate Program, University of Iowa, Iowa City, IA

[3]Iowa Neuroscience Institute, University of Iowa, Iowa City, IA

[4]Carver College of Medicine, University of Iowa, Iowa City, IA

*To whom correspondence should be addressed:

Marco M. Hefti, MD

25 S Grand Ave MRC-108-A

Iowa City, IA 52240

(319)-335-8427

marco-hefti@uiowa.edu

ABSTRACT

Introduction: Astrocytic tau aggregates are seen in several primary and secondary tauopathies, including progressive supranuclear palsy, corticobasal degeneration, and chronic traumatic encephalopathy. In all cases, astrocytic tau consists exclusively of the longer (4R) tau isoform, even when adjacent neuronal aggregates consist of a mixture of 3- and 4R tau, as in chronic traumatic encephalopathy. The reasons for this and the mechanisms by which astrocytic tau aggregates form remain unclear.

Methods: We used a combination of RNA *in situ* hybridization and immunofluorescence in human post-mortem brain tissue and tau uptake studies in human stem-cell-derived astrocytes to determine the origins of astrocytic tau in 4R tauopathies.

Results: We found that astrocytes in 4R tauopathies do not upregulate tau mRNA expression, either comparing all astrocytes between disease or tau positive- and negative astrocytes within diseases. We then found that stem-cell-derived astrocytes preferentially take up long isoform (4R) labeled recombinant tau and that this uptake is impaired by inflammation or nutritional stress. Astrocytes exposed to either 3R or 4R tau also showed downregulation of genes related to astrocyte differentiation.

Discussion: Our findings suggest that astrocytes preferentially take up neuronal 4R tau from the extracellular space, which potentially explains why astrocytic tau aggregates contain only 4R tau, and that tau uptake is impaired by decreased nutrient availability or neuroinflammation, both of which are common in the aging brain.

Introduction:

Neurodegenerative tauopathies can be classified based on the composition of pathological tau aggregates into pure short (3R) isoform, mixed, and pure long (4R) isoform. Interestingly, only 4R tauopathies, such as corticobasal degeneration (CBD) or progressive supranuclear palsy (PSP), develop astrocytic tau pathology. Tau pathology in Pick's disease, a pure 3R tauopathy, and mixed tauopathies such as Alzheimer's disease (AD) is limited to neurons. Even in chronic traumatic encephalopathy, where the pathognomonic neuronal tau aggregates in the depths of sulci are composed of a mixture of 3R and 4R tau, astrocytic tau aggregates are pure 4R (Cherry et al., 2020). In rodent models, astrocytic tau cannot propagate in the absence of neuronal tau expression (Narasimhan et al., 2020), and human single-cell sequencing and RNA *in situ* hybridization data do not show an upregulation of tau expression in astrocytes from PSP patients (Forrest et al., 2023; Sharma et al., 2021). The human studies are, however, based on small numbers of cases, and corticobasal degeneration, which also has astrocytic tau aggregates, has not been systematically studied. Astrocytes readily take up both filamentous and monomeric recombinant tau *in vitro* (Heidi et al., 2018; Juan Ramón et al., 2019; Wang and Ye, 2021), but the ability of astrocytes to take up different tau isoforms (e.g., 3R vs. 4R) remains largely unknown. Here, we report the first systematic assessment of astrocytic tau expression in human brain tissue across multiple neurodegenerative disorders and the novel findings that astrocytes preferentially take up 4R tau monomers, which is impaired by exposure to inflammatory or nutritional stress.

RESULTS:

Astrocytic tau in human primary tauopathies is of neuronal origin. We first sought to determine whether astrocytes in primary tauopathies, such as corticobasal degeneration and progressive supranuclear palsy, increase their expression of tau mRNA. Using combined RNA

in situ hybridization (RNAscope) and immunofluorescence, we found that the mean number of MAPT (tau) mRNA puncta per astrocyte (defined by positive immunofluorescence for GFAP) **(Fig. 1a)** and the number of astrocytes with puncta (**Fig. 1b)** did not differ significantly between adult control, Alzheimer disease, PSP, and CBD. We then sought to determine whether astrocytes containing tau aggregates ($GFAP^+AT8^+$) had higher levels of tau mRNA than those without. Comparing $GFAP^+AT8^+$ to $GFAP^+AT8^-$ astrocytes *within* cases with progressive supranuclear palsy (PSP), we found no statistically significant difference in the mean number of puncta per astrocyte (**Fig. 1c**) or in the number of astrocytes expressing tau mRNA (not shown).

hESC-derived astrocytes preferentially take up 4R tau. We then sought to characterize the ability of astrocytes to take up 3R and 4R tau using labeled recombinant tau and human stem-cell-derived astrocytes. Stem cells and all subsequent differentiation steps were validated using a combination of immunocytochemistry (**Fig. 2, and S1-S3)** and trilineage differentiation (**Fig. S4)**. Recombinant tau produced in *E. coli* was validated by SDS-PAGE, followed by Coomassie Blue staining and western blotting (**Fig. S5a** and **S5b,** respectively). When cultured with Cy5-labeled recombinant 1N3R or 1N4R tau, astrocytes took significantly more 4R than 3R tau ($p<10^{-4}$), with 4R uptake occurring earlier than 3R (**Fig. 3).** This result was independently validated with a separate, independently differentiated, batch of astrocytes (**Fig. S6)**.

Astrocytic tau uptake impairs astrocyte maturation. We then use bulk RNA sequencing to characterize the effect of 3R and 4R monomer uptake on astrocytes. We found 60 genes that differed between 3R and control, 29 between 4R and control, and no differentially expressed genes between 3R and 4R uptake. Nine genes were significantly downregulated in both the 3R and 4R-exposed conditions compared to controls (**Fig. 4**). Five genes showed significant downregulation by at least a factor of two in both comparisons (C4orf48, HES4, INAFM1, TMEM59L, CAMK2N2). Of these down-regulated genes, C4orf48, HES4, INAFM1, and

TMEM59L promote stem cell or astrocyte differentiation, which suggests that tau uptake impairs astrocyte differentiation (Aoki et al., 2014; Endele et al., 2011; Fleck et al., 2022).

Astrocytes exposed to inflammatory or nutritional stress have impaired tau uptake and degradation. We then sought to test the effect of two distinct models of astrocytic stress on astrocytic tau uptake and degradation. We chose to focus on serum starvation, a model of nutritional stress, and an A1 reactive astrocyte model using TNF-alpha, IL1-alpha, and C1q ("TIC") (Liddelow et al., 2017). The two models showed identical results, with both taking up significantly less 4R tau than their control counterparts (TIC vs. control, p=0.0015 and serum starved vs. control, p=0.0005) (**Fig. 5**). The amount of tau taken up between reactive astrocyte conditions, however, was not significantly different (**Fig. 5**).

Discussion:

Our data shows that astrocytes do not increase tau expression in progressive supranuclear palsy or corticobasal degeneration. This is true *between* cases, when PSP or CBD are compared to controls, and *within* cases, comparing tau-positive and negative astrocytes in patients with PSP. We then went on to show that stem cell-derived astrocytes preferentially take up 4R rather than 3R tau, that this downregulates the expression of genes related to astrocyte differentiation and is impaired by nutritional or inflammatory stress.

Our findings are broadly in agreement with single nuclear sequencing and RNA *in situ* hybridization studies in progressive supranuclear palsy (Forrest *et al.*, 2023; Sharma *et al.*, 2021). Our work is complementary to and builds on that presented by Forrest et al in that we include a larger number of cases, use GFAP immunofluorescence to better identify astrocytic mRNAs, and include a larger number of cases. We also examined astrocytic tau expression in AD and CBD, which have not been previously characterized in histologic sections. Our findings are also complementary to work by other groups showing that astrocytes take up both tau

monomers and oligomers (Heidi *et al.*, 2018; Juan Ramón *et al.*, 2019; Wang and Ye, 2021). Our findings support and build on this data by demonstrating isoform-specific uptake of tau monomers, which has, to our knowledge, not been previously described.

Our studies are limited by the low throughput of our RNA *in situ* assays and downstream analytic pipeline, which limits the number of cases examined, and by the small number of channels available in our RNAscope workflow. We were also not able to determine whether there is a difference in tau expression between tau-positive and negative astrocytes in corticobasal degeneration. This is due to the more diffuse nature of astrocytic plaques compared to the tufted astrocytes seen in PSP and the resulting difficulty in identifying the parent astrocytes in our thin (5 μm) sections. Answering this question will require three-dimensional reconstruction in thicker sections or the application of tissue-clearing methods. Novel spatial transcriptomic methods combined with protein stains to identify tau-positive astrocytes also show great promise for in-depth astrocytic phenotyping in PSP and CBD. Our uptake assays are inherently limited due to their reliance on recombinant tau monomers which do not necessarily recapitulate the post-translational modification patterns seen in the human brain. The relative toxicity of tau monomers and oligomers and their respective contributions to astrocytic tau pathology likewise remains unknown.

In summary, we have shown that astrocytes in PSP and CBD do not upregulate tau expression, that they preferentially take up 4R tau monomers *in vitro*, and that this process is impaired by nutritional and inflammatory stress. These findings strongly suggest that the increased levels of astrocytic tau seen in PSP and CBD are due to neuronal uptake rather than to the upregulation of astrocytic tau production and identify a potential mechanism for the isoform-selectivity of astrocytic tau aggregates. Future studies will be necessary to determine the molecular mechanisms for this uptake and its downstream effects on the recipient astrocytes.

Methods:

Resource availability.

Corresponding author: Marco M. Hefti, MD

Materials availability: The TauE and TauB plasmids are available through AddGene.

Data availability: All data generated in this project are included in the manuscript or its associated supplementary data files.

Code availability: The code created for this project is included in the supplementary materials.

Tissue procurement*.* Formalin-fixed paraffin-embedded (FFPE) tissue was obtained as previously described (Fiock et al., 2023). Individual cases used, demographic information, and sources are listed in **Table 1.** The University of Iowa's Institutional Review Board determined that, since this project used tissue from deceased individuals exclusively, it does not represent human subjects research under the NIH common rule (determination #201706772). All methods were conducted in accordance with the relevant laws, regulations, guidelines, and ethical standards of our institution and with the 1964 Helsinki declaration and its later amendments or comparable ethical standards. Diagnoses were made according to the updated National Alzheimer's Coordinating Center neuropathologic diagnostic criteria and other published guidelines (Armstrong et al., 2013; Dickson et al., 2002; Dickson et al., 2011; Hoglinger et al., 2017; Montine et al., 2012).

Combined RNA in situ Hybridization and Immunofluorescence*.* RNA *in situ* hybridization (RNAscope) with immunofluorescence (IF) was performed for FFPE tissue using the 3-plex Multiplex Fluorescent v2 Reagent Kit (Cat No. 323100, ACDBio) with a MAPT probe (Cat. No 408991, ACDBio) according to the manufacturer's instructions and as previously described (Fiock *et al.*, 2023). Baking, deparaffinization, and H_2O_2 treatment were done as above for Basescope. Target retrieval was performed using a vegetable steamer for 15 minutes at 85°C,

followed by Protease Plus treatment (Cat No. 322330, ACDBio) for 30 minutes at 40°C in a HybEZ Oven (above). The probes were hybridized for 2 hours at 40°C in the HybEZ Oven. The slides were then stored in 5X SSC (20X SSC Cat No. V4261, Promega) overnight. Amplification and detection were performed following the manufacturer's instructions, using the Cyanine 5 TSA fluorophore (NEL745E001KT, Perkin Elmer) at 1:400.

For the immunofluorescence staining, slides were washed using TBST made using 10X TBS (Cat No. 1706435, Bio-Rad) and 0.05% Tween20 (Cat No. 9005-64-5, Sigma Aldrich). Slides were blocked in 10% normal goat serum (Cat No. 31873, Thermo Fisher) diluted in 1X TBS and 0.1% Bovine Serum Albumin (BSA; Cat No. 9048-46-86, RPI) for 30 minutes at room temperature. Slides were incubated with primary antibodies for GFAP and AT8 (diluted 1:1000 in TBS + 0.1% BSA) for 1.5 hours in a humidified chamber at room temperature followed by three five-minute TBST washes (Table 2). Goat anti-mouse IgG H&L Alexa Fluor® 555 and goat anti-rabbit IgG H&L Alexa Fluor® 488 were diluted 1:1000 in TBS + 0.1% BSA, and slides were incubated for 30 minutes in a humidified slide chamber at room temperature protected from light (Table 2). After washing three times for 2 minutes in TBST, autofluorescence quenching was done using TrueBlack Lipofuscin Autofluorescence Quencher diluted according to manufacturer's guidelines (23007, Biotium) for 30 seconds followed by DAPI and coverslipping with VectaShield Plus antifade mounting medium (H-1900, Vector Labs). Appropriate controls were run with the 3-plex positive (Cat. No 320861, ACDBio) and 3-plex negative (Cat. No 320871, ACDBio) control probes for RNAscope, as well as an IF-only control to detect any false positive or false negative results (Figure 7). We have previously validated the MAPT probe using human tau transgenic mice (Fiock et al., 2020).

Slide Scanning and Quantification. Slide scanning and quantification were done using a Cytation 5 from Agilent (above) with GEN5PRIME software (above) to create a customized protocol. Each set of experiments was run using identical protocol settings. A discovery scan

was done to image the entire piece of tissue at 4X (above) using a combination of the DAPI filter cube (Cube: Cat No. BT1225100, Agilent; LED: Cat No. BT1225007, Agilent), GFP filter cube (Cube: Cat No. BT1225101, Agilent; LED: Cat No. BT1225001, Agilent), TRITC filter cube (Cube: Cat No. BT1225125, Agilent; LED: Cat No. BT1225012, Agilent), and CY5 filter cube (Cube: Cat No. BT1225105, Agilent; LED: Cat No. BT1225005, Agilent) as appropriate. Five regions of interest (ROIs) were selected at random in the cortex for each tissue using approximately equal sized ROIs; then each ROI was imaged in the appropriate channels using the above filters at 40X (Cat No. BT1320518, Agilent) and stitched using the GFP channel as a reference with 150μm of overlap.

For quantification, subpopulations were defined in GEN5PRIME to identify cell types of interest and count the number of RNA puncta present. Astrocytes were defined as cells with a nucleus size of less than 15 based on DAPI and a mean GFP intensity of at least 10,000; astrocytes with tau pathology were defined as cells that met the above criteria in addition to a mean TRITC intensity of at least 10,000, and astrocytes without tau pathology were defined as cells that met the above criteria with a mean TRITC intensity of less than 10,000. RNA puncta were counted in each population based on the size of puncta (between 2-5μm) using either the CY5 channel alone or the TRITC and CY5 channels as appropriate. The average number of puncta in each subpopulation was calculated by GEN5PRIME using all five ROIs for each slide. P-values were assessed in GraphPad Prism using t-tests with each sample counting as one biological replicate, and graphs were made using R Studio and Adobe Illustrator. Data is presented as mean ± standard error of the mean (SEM).

Stem cell procurement and culture. The H14 human embryonic stem cell (hESC) line was obtained from WiCell (Cat No. WAe014-A) and is listed as an NIH-approved line for research purposes (NIH Approval Number: NIHhESC-10-0064). Stem cell culture was done using a commercially available media kit (mTeSR Plus; Cat No. 100-0276, STEM CELL Technologies)

following the manufacturer's published protocol (Figure 8) (Technologies, 2020). Briefly, cell colonies were grown on Matrigel-coated 6-well plates (Matrigel: Cat No. 354277, Corning; Plates: Cat No. CLS3516-50EA, Sigma Aldrich) in mTeSR Plus for at least three passages before being dissociated for downstream differentiation protocols. Matrigel was diluted according to the lot-specific dilution factor recommended by the manufacturer in 25 ml of DMEM/F12 HEPES (Cat No. 36254, STEMCELL Technologies) and set for 1 hour at 37°C before plates were used. Areas of cellular differentiation were removed each day from cultures. Passaging of colonies was done roughly every five days using Gentle Cell Dissociation Reagent (GCDR) from STEMCELL Technologies (Cat No. 100-0485). Stem cell pluripotency was validated using the STEMdiff Trilineage Differentiation Kit (STEMCELL Technologies, Cat No. 05230) and human stem cell antibody array from AbCam (Cat No. ab211066) according to the manufacturer's directions.

Generation of neural progenitor cells. Neural progenitor cells (NPCs) were created from the hESCs described above using the STEMdiff SMADi Neural Induction kit from STEMCELL Technologies (Cat No. 08581) according to their guidelines for Matrigel-coated 6-well plates (Figure 8) (Technologies, 2021b). Briefly, colonies were checked for areas of differentiation and removed, if necessary, before washing once with cold DPBS-/-. Colonies were then incubated for 8-10 minutes at 37°C in GCDR for dissociation. Cells were collected and triturated to create a single-cell suspension, then spun down at 300g for 5 minutes at room temperature. Cell counts were determined using a Countess 3 instrument (Cat No. AMQAX2000, Thermo Fisher), and 2,000,000 cells/well were plated in a 6-well plate in STEMdiff SMADi Neural Induction media. Daily media changes were performed for seven days followed by passaging of progenitor cells using Accutase (Cat No. 07920, STEMCELL Technologies), which was repeated for one additional passage (two passages total). Cells were plated at 1,500,000 cells/well in a 6-well plate for each passage. At passage 3, cells were either frozen down in CryoStor CS10 (Cat

No. 07930, STEMCELL Technologies) at 3,000,000 cells/vial or moved onto the next step of the differentiation process.

Astrocyte Precursor Cells and Mature Astrocytes. Astrocyte precursor cells were created from the neural progenitor cells described above using the STEMdiff Astrocyte Differentiation media kit from STEMCELL Technologies (Cat No. 100-0013) following their protocol for Matrigel-coated 6-well plates (Technologies, 2021a). Briefly, progenitor cells were plated at a seeding density of 1,900,000 cells/well in a Matrigel-coated 6-well plate and given daily media changes for seven days. For passaging, cells were incubated with Accutase for 8-10 minutes at 37°C then spun down at 400g for 5 minutes at room temperature. Cell counts were obtained using a Countess 3 instrument, and a density of 1,400,000 cells/well was used. Media changes were performed every other day for seven days, then the process was repeated once more (seeding density: 1,600,000 cells/well) for a total of two passages in the differentiation media. At passage 3, precursor cells were either frozen in CryoStor CS10 (above) at 2,000,000 cells/vial or moved onto the final stage of differentiation.

Mature astrocytes were created from astrocyte precursor cells using the STEMdiff Astrocyte Maturation media kit from STEMCELL Technologies (Cat No. 100-0016) following their guidelines for Matrigel-coated 6-well plates. Briefly, precursor cells were seeded at 1,900,000 cells/well in a 6-well plate, and media changes were performed every other day for seven days. Cells were dissociated with Accutase for 8-10 minutes at 37°C before being spun down at 400g for 5 minutes at room temperature. This process was repeated once more for 2 passages in the maturation media before cells were plated for downstream analysis.

Immunocytochemistry. Primary and secondary antibodies used with their respective concentrations are shown in **Table 2.** Cells for ICC were grown in a 12-well plate (Cat No. 3513,

Costar) on autoclave-sterilized 18mm coverslips (Cat No. 12545100, Fisher Scientific) coated with Matrigel using the same protocol as described above. Coverslips were washed once with 1X PBS before fixing for 30 minutes with 10% formalin at room temperature and were subsequently washed twice with 1X PBS before storing in 1X PBS+ 0.01% sodium azide at 4°C. Coverslips were placed in a 12-well plate and incubated for 10 minutes at room temperature in extraction solution (0.02% Triton-X 100 in 1XPBS; Triton-X 100: Cat No. BP151, Fisher Scientific) before blocking for 30 minutes at room temperature in blocking solution (10% heat-inactivated fetal bovine serum (hiFBS) in 1XPBS; hiFBS: Cat No. S1245914, R&D Systems). Primary antibody incubation was done with the respective antibodies diluted in serum solution (1% hiFBS in 1XPBS) overnight at 4°C with gentle rocking. Coverslips were washed five times for 1 minute each at room temperature with 1X PBS, then incubated in secondary antibody diluted in serum solution for 1 hour at room temperature protected from light with gentle rocking. Five 1-minute 1X PBS washes were performed before incubation with TrueView Autofluorescence Quenching solution (prepared according to manufacturer's guidelines and diluted 1:10 with ddH_2O) for 5 minutes with gentle agitation at room temperature protected from light. Coverslips were washed once more for 5 minutes with 1X PBS at room temperature with the addition of three drops of DAPI (Cat No. R37606, Invitrogen) then mounted on SuperFrost Plus slides (Cat No. 12-550-15, Fisher Scientific) using VECTASHIELD Plus mounting medium (Cat No. H-1900, Vector Laboratories).

Generation of plasmids. Custom human TauB and TauE plasmids were created on a pET29b backbone by GenScript on a fee-for-service basis, with 6xHIS and S tags added to the N- and C-terminal ends to ensure high purity of the resulting protein preparations. The resulting plasmids were validated by long-read sequencing (Plasmidsaurus), transformed into BL21 (DE3) OneShot Competent Cells (Cat No. C6000-03, Life Technologies), and given to the

Carver College of Medicine's Protein and Crystallography Facility at the University of Iowa for recombinant protein generation.

Generation of recombinant tau. Recombinant human TauB (1N3R) and TauE (1N4R) proteins were produced at the Carver College of Medicine's Protein and Crystallography Facility at the University of Iowa. Protein was produced in *E. coli* BL21 (DE3) cells (Cat No. 69450, Novagen) with the pET29b plasmids generated above. Bacteria were grown in Luria Broth (Cat No.910-79-40-2, Research Products International) in the presence of kanamycin (100 ug/mL), and protein overexpression was induced with 1 mM IPTG in 3 hours at 37°C. Cells were disrupted by sonication and boiled at 75°C for 15 minutes in buffer (50 mM $NaPO_4$, 2 mM EDTA and 2 mM DTT, pH 6.8). All subsequent procedures were performed at 4°C. Lysate was ultracentrifuged at 80,000g for 45 minutes, and protein was purified by cation exchange chromatography (HiTrap SP, GE Healthcare), followed by size exclusion chromatography (HiLoad 16/600 Superdex 200 pg, GE Healthcare). Recombinant tau was labeled using an Alexa Fluor 647 Protein Labeling Kit (Invitrogen, Cat No. A20173) with 500 mg of recombinant protein input at a concentration of 1 mg/mL according to the manufacturer's recommendations. Successful labeling was confirmed by measuring absorbance on a NanoDrop spectrophotometer.

Western blotting. Western blots were run using 20 ng of purified protein or xxx μg of cell lysate. Samples were run on a 10% Mini-PROTEAN TGX Stain-Free Precast gel (Cat No. 4561036, Bio-Rad) and blotted to PVDF. The membrane was blocked in EveryBlot blocking buffer (Cat No. 12010020, Bio-Rad) for 10 minutes at room temperature, then HT7 was diluted 1:5000 in EveryBlot and incubated with the membrane overnight at 4°C (Table 2). Horseradish peroxidase-labeled horse anti-mouse secondary was used at 1:5000 diluted in EveryBlot for 1 hour at room temperature and detected by Clarity Western ECL substrate (Cat. No 1705060,

Bio-Rad) (Table 2). Chemiluminescence was measured using a ChemiDoc Touch Imaging System (above).

Astrocyte plating for live cell imaging. Mature astrocytes were plated in glass bottom 12-well plates (Cat No. P12-1.5H-N, Cellvis) at a density of 200,000 cells/well and allowed to settle for a minimum of 24 hours before live-cell imaging. For experiments requiring different media conditions, cells were plated in either STEMDiff Astrocyte Maturation media without Supplement B (serum-starved) or STEMDiff Astrocyte Maturation media without Supplement B with the addition of "TIC" proinflammatory factors (30ng/mL TNF-alpha (Cat No. 300-01A-10ug, Peprotech), 3ng/mL IL1-alpha (Cat No. 500-P21A-50ug, Peprotech), 400ng/mL C1q (Cat No. ab282858, Abcam) (TIC) (Labib et al., 2022). Serum starvation occurred either at the beginning of the astrocyte maturation protocol (three weeks total) or for four days before live-cell imaging, and "TIC" induction occurred 24 hours prior to live-cell imaging.

Live cell imaging. Live-cell imaging was done using a Cytation 5 (above) with GEN5PRIME software (above) for either 24- or 48 hours using phase contrast with laser autofocus (Cat No. BT1225010, Agilent) and the CY5 filter cube (above) at 20X (Cat No. BT1320517, Agilent). Cells were incubated in the imager at 37°C with 5% CO_2 to mimic normal incubator conditions. A 5x5 matrix was used to capture 25 tiles across the center of the well with images captured every hour throughout the experiment. Images were processed in GEN5 to remove background fluorescence in the CY5 channel caused by phenol red in the media then tau puncta spots were counted by GEN5 using a minimum and maximum size cutoff (2.5μm and 10μm, respectively). Due to difficulties counting cells on phase contrast by GEN5, all phase contrast images for timepoint 1 (baseline) in each experiment were imported into Labscope (Zeiss). Cells were counted using the default settings of the AI Cell Counting Module (Zeiss), and counts were exported into a spreadsheet for data analysis.

RNA sequencing. RNA extraction was performed from the mature hESC-derived astrocytes grown as a monolayer and used for live-cell imaging. Invitrogen's PureLink RNA Mini kit (Cat No. 12183018A) was used for RNA extraction according to the manufacturer's protocol, and samples were sent to GeneWhiz for sequencing. For samples sent as cell pellets, cells were grown as described above, then scraped into cold DPBS-/- (above) using a cell spatula and spun down at 400g for 5 minutes at 4°C. The supernatant was discarded, and pellets were flash-frozen in a dry ice/ethanol slurry. RNA extraction and sequencing were done by GeneWhiz's sequencing facility on a fee-for-service basis. Data analysis was conducted as previously described (Shin et al., 2022). Briefly, RNA sequencing reads were aligned to the hg38 human reference genome using STAR aligner. Reads were quantified using the *subreads* package, and comparative gene expression analysis was done using the *DESeq2* package in R. Gene ontology enrichment analysis was done using the web interface from the Gene Ontology Consortium with the biological process as the readout on all significant genes ($p<0.05$) (Ashburner et al., 2000).

Statistical Analysis. Data analysis for RNA sequencing is described above. For other studies, data analysis was done by either a generalized linear model with a HAC correction for time dependence or using paired or unpaired t-tests, as appropriate. Total cell count, treatment group, and position in well were also included as independent variables for the generalized linear model. Generalized linear models were run in MATLAB, t-tests were done in GraphPad Prism, and graphs were generated using either R studio or GraphPad Prism.

Tables

Table 1. Demographic information and source of all human tissue samples used in current study.

Table 2. Antibodies used in study.

Figure 1. Astrocytes do not upregulate tau mRNA in astrocytic tauopathies. (A) Proportion of tau mRNA positive astrocytes in control, AD, PSP, and CBD. (B) Mean number of mRNA puncta per astrocyte in control, AD, PSP, and CBD. (C) Mean number of puncta comparing tau-positive and negative astrocytes within cases of PSP. (D) Representative low power ROI with insets of tau-positive and negative astrocytes shown in (E) and (F), respectively. Scale bars = 1000 μm in (D) and 20 μm in (E) and (F).

Figure 2. Validation of cell differentiation. (A) Stem cells show positive staining for OCT4 and NANOG, (B) neuronal precursor cells positive for Nestin, SOX1, and PAX6. (C) astrocyte staining for S100β and GFAP, (D) S100β and DCX. A single cell showing neuronal differentiation is indicated by white arrow in (D). Scale bars = 200 μm. Individuals panels for each stain are shown in **Figs. S1, S2,** and **S3** for stem cells, neural progenitors, and astrocytes, respectively.

Figure 3. hESC-derived astrocytes preferentially take up 4R tau. hESC-derived astrocytes exposed to either labeled recombinant 3R or 4R tau over the course of 24 hours exhibit preferential uptake of 4R. *$p<10^{-4}$ Image stills of hESC-derived astrocytes exposed to labeled recombinant 3R or 4R tau (magenta) over the course of 24 hours show more 4R in cells than 3R. Scale bar = 200μm

Figure 4. Effect of 3R and 4R tau uptake on astrocyte transcriptome. Volcano plots showing differentially expressed genes between 3R and control (A), 4R and control (B), and 3R and 4R (C). Genes differentially expressed in both 3R and 4R are shown in (D). Grey lines in (A) – (C) indicate cutoffs of adjusted p-value > 0.05 (horizontal) and absolute fold change > 2.

Figure 5. Nutritional or inflammatory stress impairs astrocyte tau uptake. hESC-derived astrocytes exposed to labeled 4R tau with or without serum starvation (SS) or TIC protocol (TNFα, IL-6, C1q) with representative still images.

Figure S1. Validation of stem cells by immunocytochemistry. Channels shown separately for image in **Fig. 2**. Scale bar = 200 μm.

Figure S2. Validation of neural progenitor cells by immunocytochemistry. Channels shown separately for image in **Fig. 2**. Scale bar = 200 μm.

Figure S3. Validation of astrocyte differentiation by immunocytochemistry. Channels shown separately for image in **Fig. 2**. Scale bar = 200 μm.

Figure S4. Additional validation of stem cell pluripotency by trilineage differentiation.

Figure S5. Validation of recombinant tau. (A) Recombinant TauE (1N4R) and TauB (1N3R) was run on an SDS-PAGE gel and stained with Coomassie Blue to assess for purity. Red box on whole gel represents magnified region shown above. (B) TauE and TauB were run on an SDS-PAGE gel, transferred to PVDF membrane and probed with anti-tau (HT7). Red box indicates relevant area magnified above.

Figure S3. Replication of Figure 3

Table S1. List of all genes for Figure 4.

REFERENCES

Aoki, M., Segawa, H., Naito, M., and Okamoto, H. (2014). Identification of possible downstream genes required for the extension of peripheral axons in primary sensory neurons. Biochem Biophys Res Commun *445*, 357-362. 10.1016/j.bbrc.2014.01.193.

Armstrong, M.J., Litvan, I., Lang, A.E., Bak, T.H., Bhatia, K.P., Borroni, B., Boxer, A.L., Dickson, D.W., Grossman, M., Hallett, M., et al. (2013). Criteria for the diagnosis of corticobasal degeneration. Neurology *80*, 496-503. 10.1212/WNL.0b013e31827f0fd1.

Ashburner, M., Ball, C.A., Blake, J.A., Botstein, D., Butler, H., Cherry, J.M., Davis, A.P., Dolinski, K., Dwight, S.S., Eppig, J.T., et al. (2000). Gene ontology: tool for the unification of biology. The Gene Ontology Consortium. Nat Genet *25*, 25-29. 10.1038/75556.

Cherry, J.D., Kim, S.H., Stein, T.D., Pothast, M.J., Nicks, R., Meng, G., Huber, B.R., Mez, J., Alosco, M.L., Tripodis, Y., et al. (2020). Evolution of neuronal and glial tau isoforms in chronic traumatic encephalopathy. Brain Pathol *30*, 913-925. 10.1111/bpa.12867.

Dickson, D.W., Bergeron, C., Chin, S.S., Duyckaerts, C., Horoupian, D., Ikeda, K., Jellinger, K., Lantos, P.L., Lippa, C.F., Mirra, S.S., et al. (2002). Office of Rare Diseases neuropathologic criteria for corticobasal degeneration. J Neuropathol Exp Neurol *61*, 935-946. 10.1093/jnen/61.11.935.

Dickson, D.W., Kouri, N., Murray, M.E., and Josephs, K.A. (2011). Neuropathology of frontotemporal lobar degeneration-tau (FTLD-tau). J Mol Neurosci *45*, 384-389. 10.1007/s12031-011-9589-0.

Endele, S., Nelkenbrecher, C., Bordlein, A., Schlickum, S., and Winterpacht, A. (2011). C4ORF48, a gene from the Wolf-Hirschhorn syndrome critical region, encodes a putative

neuropeptide and is expressed during neocortex and cerebellar development. Neurogenetics *12*, 155-163. 10.1007/s10048-011-0275-8.

Fiock, K.L., Betters, R.K., and Hefti, M.M. (2023). Thioflavin S Staining and Amyloid Formation Are Unique to Mixed Tauopathies. J Histochem Cytochem, 221554231158428. 10.1369/00221554231158428.

Fiock, K.L., Smalley, M.E., Crary, J.F., Pasca, A.M., and Hefti, M.M. (2020). Increased Tau Expression Correlates with Neuronal Maturation in the Developing Human Cerebral Cortex. eNeuro. 10.1523/ENEURO.0058-20.2020.

Fleck, J.S., Jansen, S.M.J., Wollny, D., Zenk, F., Seimiya, M., Jain, A., Okamoto, R., Santel, M., He, Z., Camp, J.G., and Treutlein, B. (2022). Inferring and perturbing cell fate regulomes in human brain organoids. Nature. 10.1038/s41586-022-05279-8.

Forrest, S.L., Lee, S., Nassir, N., Martinez-Valbuena, I., Sackmann, V., Li, J., Ahmed, A., Tartaglia, M.C., Ittner, L.M., Lang, A.E., et al. (2023). Cell-specific MAPT gene expression is preserved in neuronal and glial tau cytopathologies in progressive supranuclear palsy. Acta Neuropathol. 10.1007/s00401-023-02604-x.

Hefti, M.M., Farrell, K., Kim, S., Bowles, K.R., Fowkes, M.E., Raj, T., and Crary, J.F. (2018). High-resolution temporal and regional mapping of MAPT expression and splicing in human brain development. PLoS One *13*, e0195771. 10.1371/journal.pone.0195771.

Heidi, M.-S., Allysa, L.C., Daniel, B.S., Dan, B.S., Fading, C., Ying-Wooi, W., Ying-Wooi, W., Ying-Wooi, W., Ying-Wooi, W., Lakshya, B., et al. (2018). TFEB enhances astroglial uptake of extracellular tau species and reduces tau spreading. Journal of Experimental Medicine. 10.1084/jem.20172158.

Hoglinger, G.U., Respondek, G., Stamelou, M., Kurz, C., Josephs, K.A., Lang, A.E., Mollenhauer, B., Muller, U., Nilsson, C., Whitwell, J.L., et al. (2017). Clinical diagnosis of progressive supranuclear palsy: The movement disorder society criteria. Mov Disord *32*, 853-864. 10.1002/mds.26987.

Juan Ramón, P., Esther, L., Esther Molina, L., José Carlos, D.-B., Jesús, A., Félix, H., Félix, H., Félix, H., Marta, B., and Marta, B. (2019). Extracellular Monomeric Tau Is Internalized by Astrocytes. Frontiers in Neuroscience. 10.3389/fnins.2019.00442.

Labib, D., Wang, Z., Prakash, P., Zimmer, M., Smith, M.D., Frazel, P.W., Barbar, L., Sapar, M.L., Calabresi, P.A., Peng, J., et al. (2022). Proteomic Alterations and Novel Markers of Neurotoxic Reactive Astrocytes in Human Induced Pluripotent Stem Cell Models. Front Mol Neurosci *15*, 870085. 10.3389/fnmol.2022.870085.

Liddelow, S.A., Guttenplan, K.A., Clarke, L.E., Bennett, F.C., Bohlen, C.J., Schirmer, L., Bennett, M.L., Münch, A.E., Chung, W.S., Peterson, T.C., et al. (2017). Neurotoxic reactive astrocytes are induced by activated microglia. Nature *541*, 481-487. 10.1038/nature21029.

Montine, T.J., Phelps, C.H., Beach, T.G., Bigio, E.H., Cairns, N.J., Dickson, D.W., Duyckaerts, C., Frosch, M.P., Masliah, E., Mirra, S.S., et al. (2012). National Institute on Aging-Alzheimer's Association guidelines for the neuropathologic assessment of Alzheimer's disease: a practical approach. Acta Neuropathol *123*, 1-11. 10.1007/s00401-011-0910-3.

Narasimhan, S., Changolkar, L., Riddle, D.M., Kats, A., Stieber, A., Weitzman, S.A., Zhang, B., Li, Z., Roberson, E.D., Trojanowski, J.Q., and Lee, V.M.Y. (2020). Human tau pathology transmits glial tau aggregates in the absence of neuronal tau. J Exp Med *217*. 10.1084/jem.20190783.

Rao, X., Huang, X., Zhou, Z., and Lin, X. (2013). An improvement of the 2^(-delta delta CT) method for quantitative real-time polymerase chain reaction data analysis. Biostat Bioinforma Biomath *3*, 71-85.

Sharma, A., Song, W.-M., Farrell, K., Whitney, K., Zhang, B., Crary, J.F., and Pereira, A.C. (2021). Single-cell atlas of progressive supranuclear palsy reveals a distinct hybrid glial cell population. bioRxiv, 2021.2004.2011.439393. 10.1101/2021.04.11.439393.

Shin, S.S., Gottschalk, A.C., Mazandi, V.M., Kilbaugh, T.J., and Hefti, M.M. (2022). Transcriptional Profiling in a Novel Swine Model of Traumatic Brain Injury. Neurotrauma Rep *3*, 178-184. 10.1089/neur.2021.0051.

Technologies, S. (2020). Maintenance of Human Pluripotent Stem Cells in mTeSR™ Plus. https://cdn.stemcell.com/media/files/manual/10000007757-Maintenance_of_Human_Pluripotent_Stem_Cells_in_mTeSR_Plus.pdf?_ga=2.55536555.1208481054.1675095773-968244009.1675095773.

Technologies, S. (2021a). Astrocyte Differentation and Maturation Manual. https://cdn.stemcell.com/media/files/pis/10000006879-PIS_06.pdf?_ga=2.263570060.1208481054.1675095773-968244009.1675095773.

Technologies, S. (2021b). Generation and Culture of Neural Progenitor Cells Using the STEMdiff™ Neural System. https://cdn.stemcell.com/media/files/manual/10000005588-Generation_Neural_Progenitor_Cells_from_hPSCs_using_STEMdiff_Neural_Induction_Medium.pdf?_ga=2.159611133.1775495983.1675356130-1992370814.1675356129.

Wang, P., and Ye, Y. (2021). Filamentous recombinant human Tau activates primary astrocytes via an integrin receptor complex. Nat Commun *12*, 95. 10.1038/s41467-020-20322-w.

A

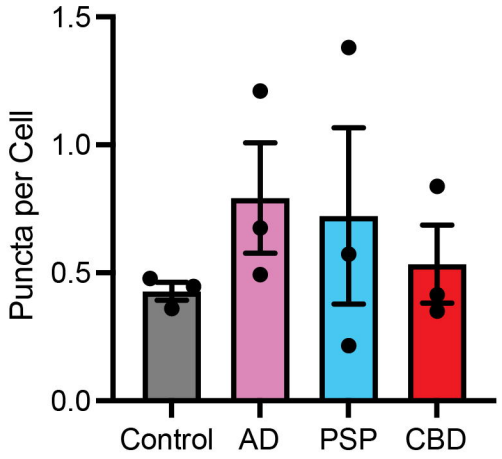
Puncta per Cell
1.5
1.0
0.5
0.0
Control
AD
PSP
CBD

B

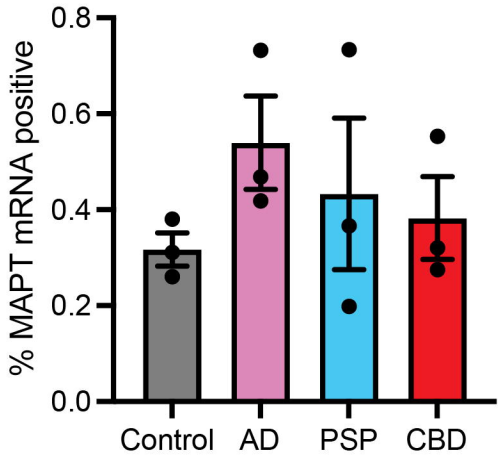
% MAPT mRNA positive
0.8
0.6
0.4
0.2
0.0
Control
AD
PSP
CBD

C

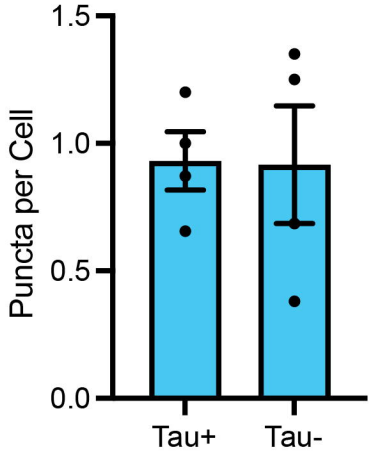
Puncta per Cell
1.5
1.0
0.5
0.0
Tau+
Tau-

D

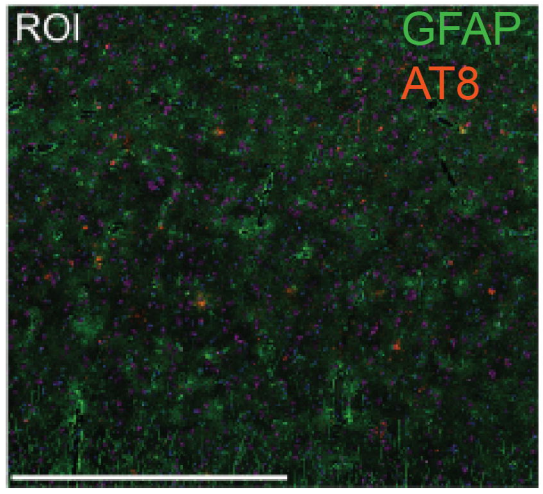
ROI
GFAP
AT8

E

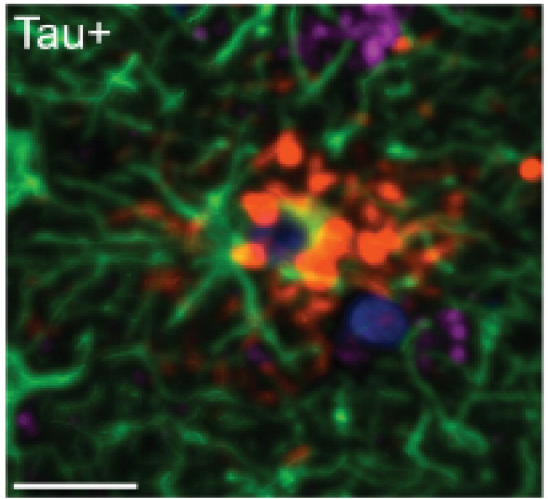
Tau+

F

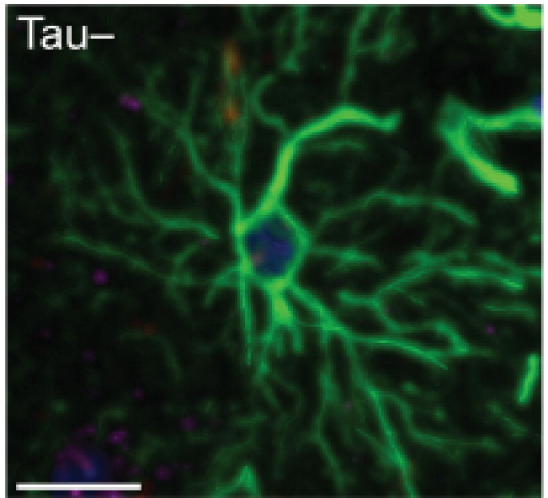
Tau–

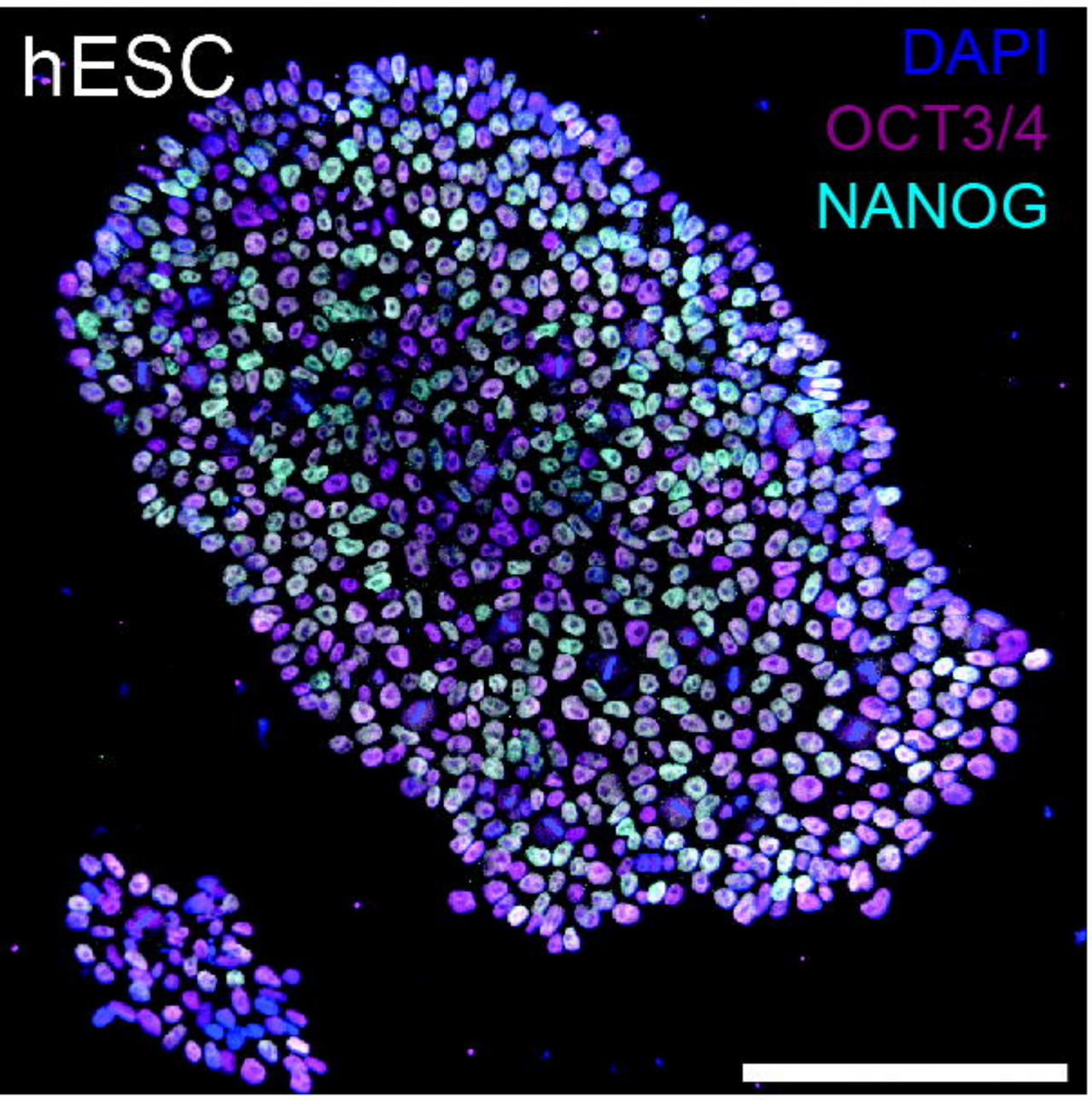
hESC
DAPI
OCT3/4
NANOG

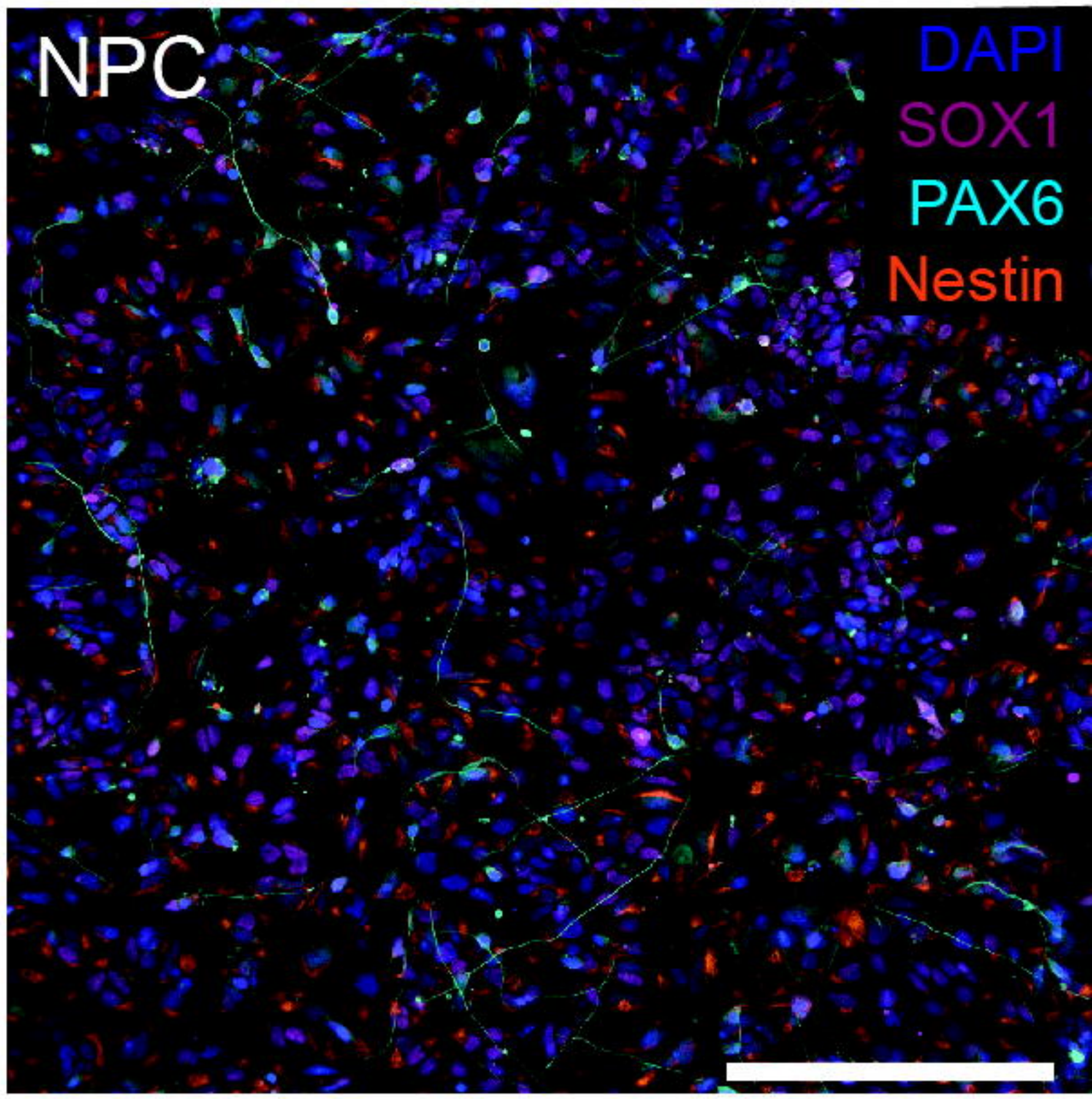
NPC
DAPI
SOX1
PAX6
Nestin

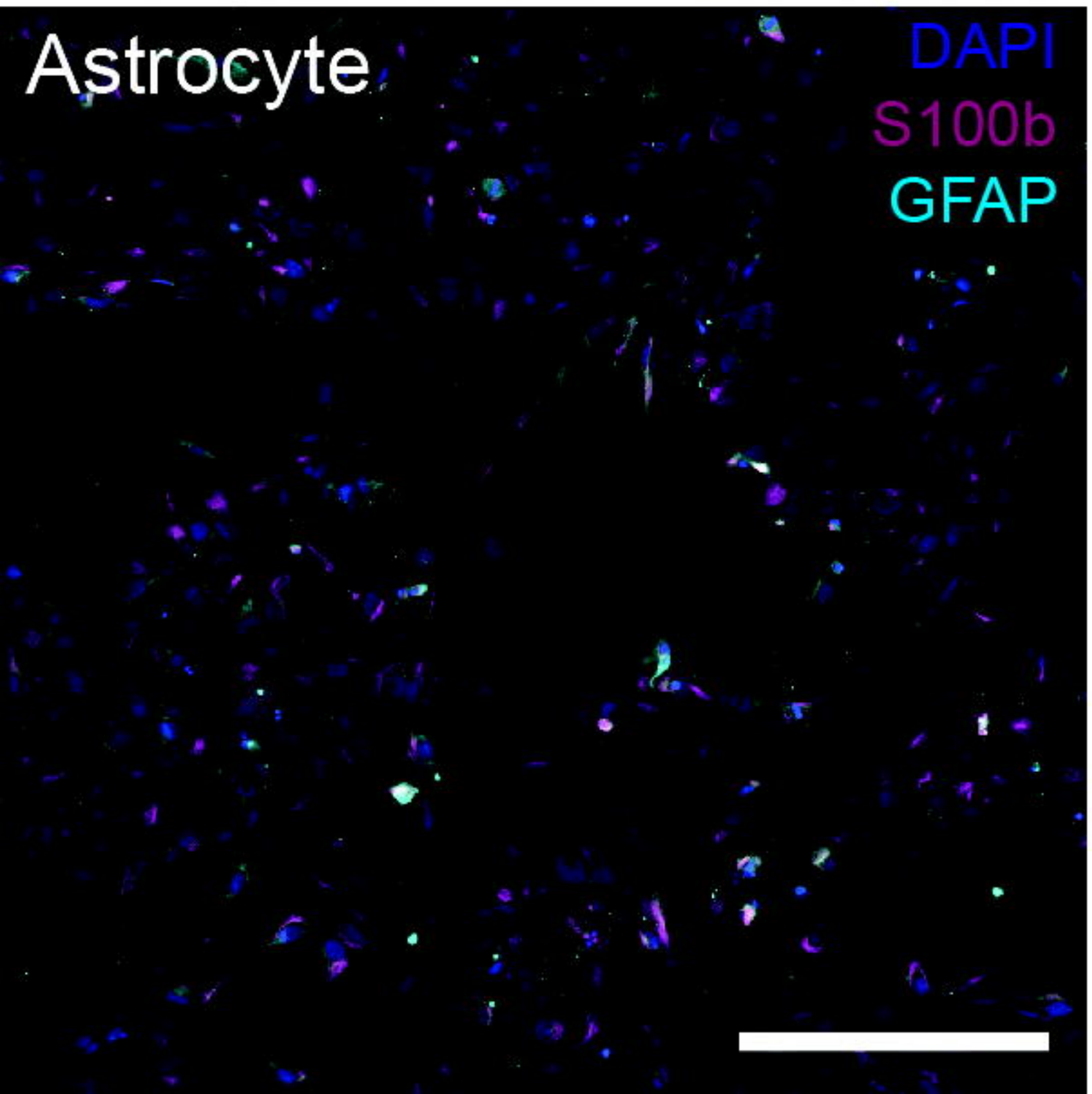
Astrocyte
DAPI
S100b
GFAP

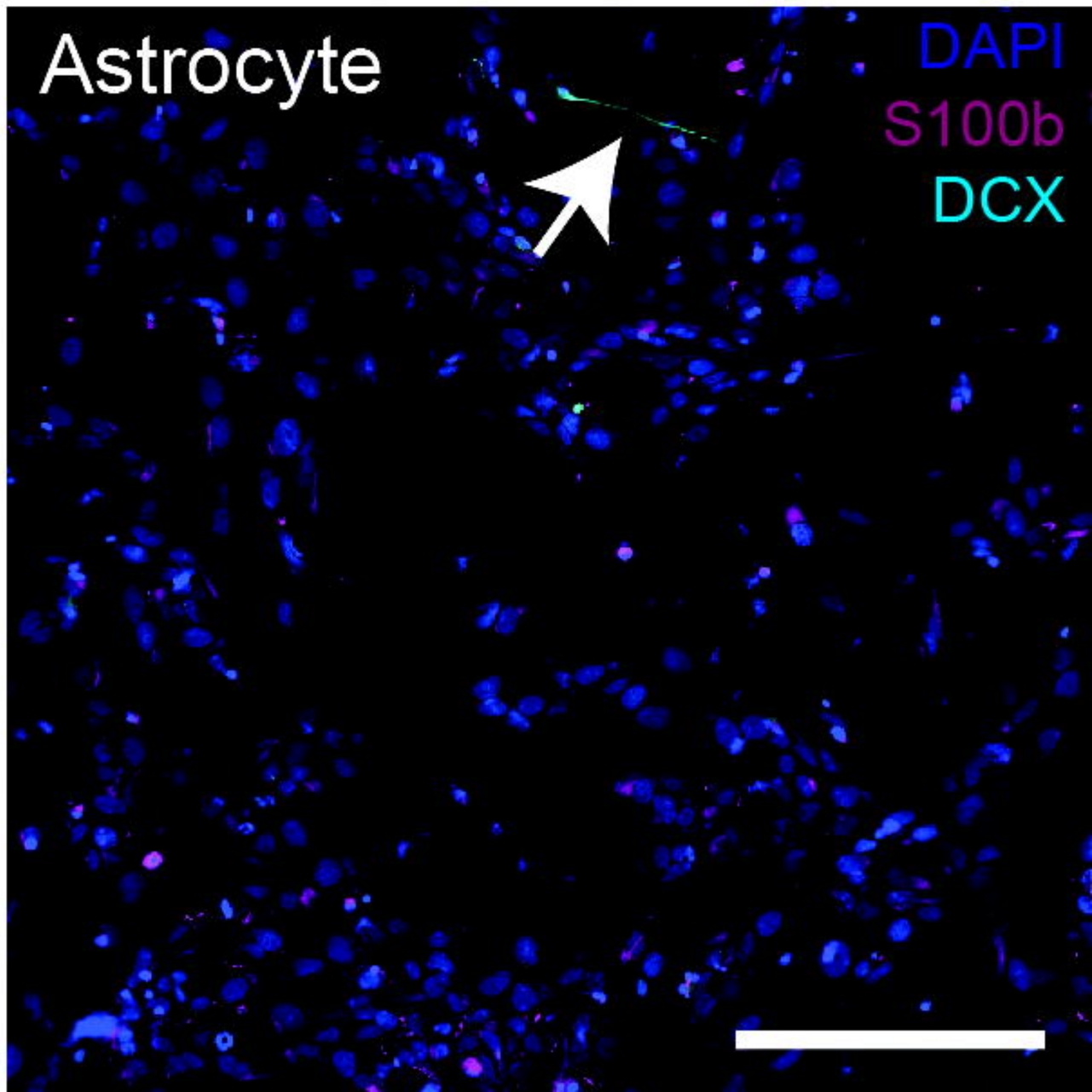
Astrocyte
DAPI
S100b
DCX

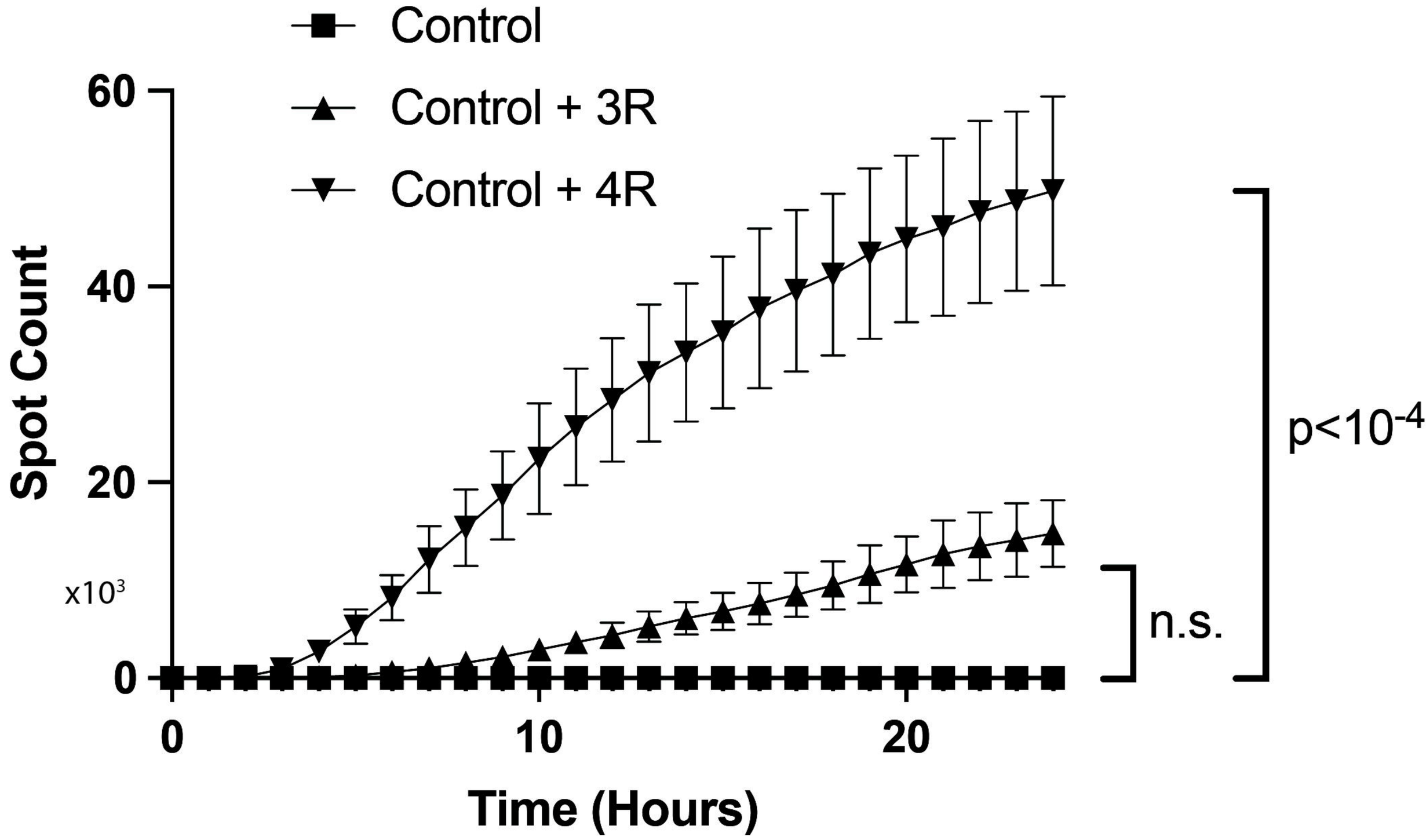
Control
Control + 3R
Control + 4R
Spot Count
x10³
60
40
20
0
0
10
20
Time (Hours)
p<10⁻⁴
n.s.

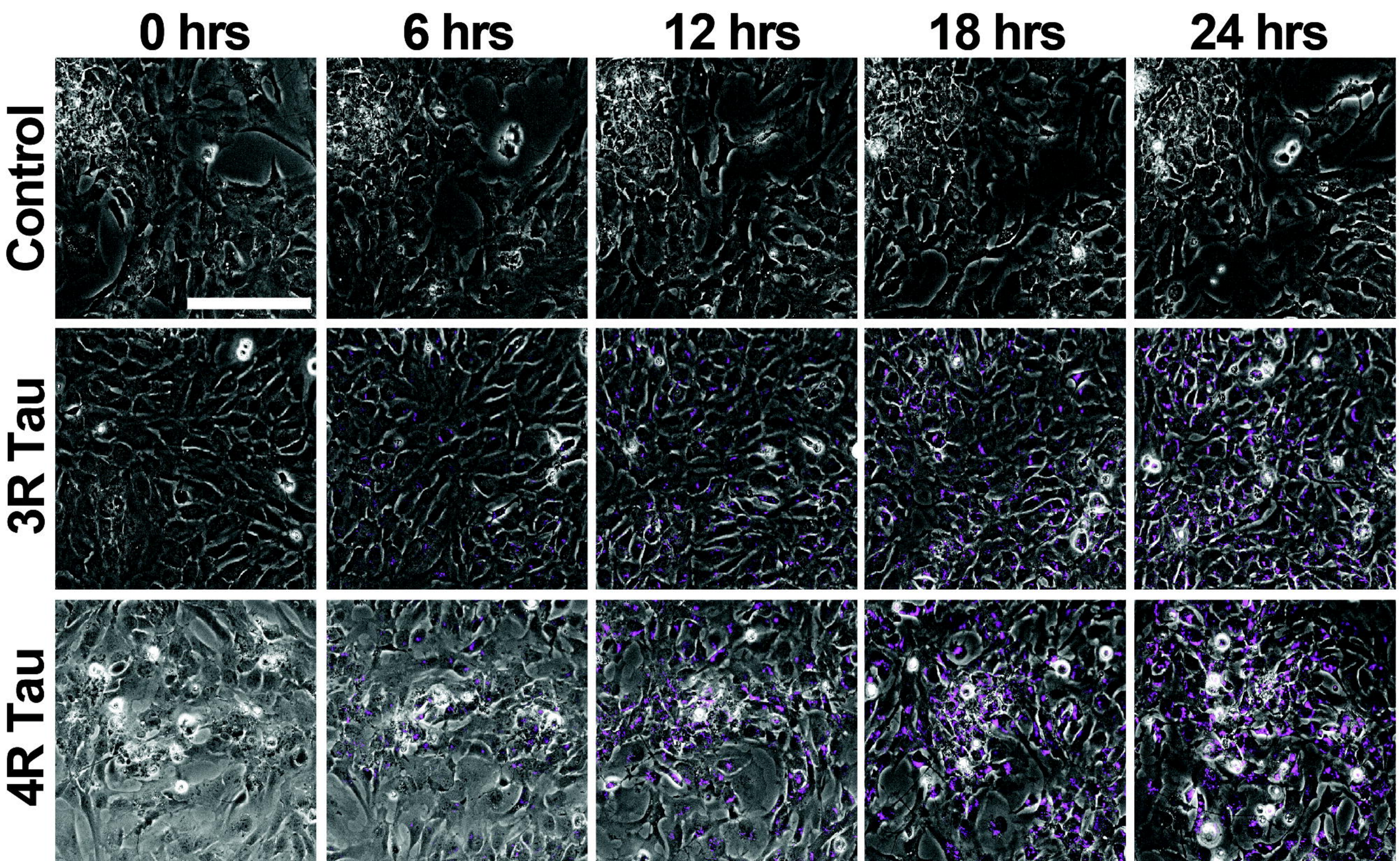
0 hrs
6 hrs
12 hrs
18 hrs
24 hrs
Control
3R Tau
4R Tau

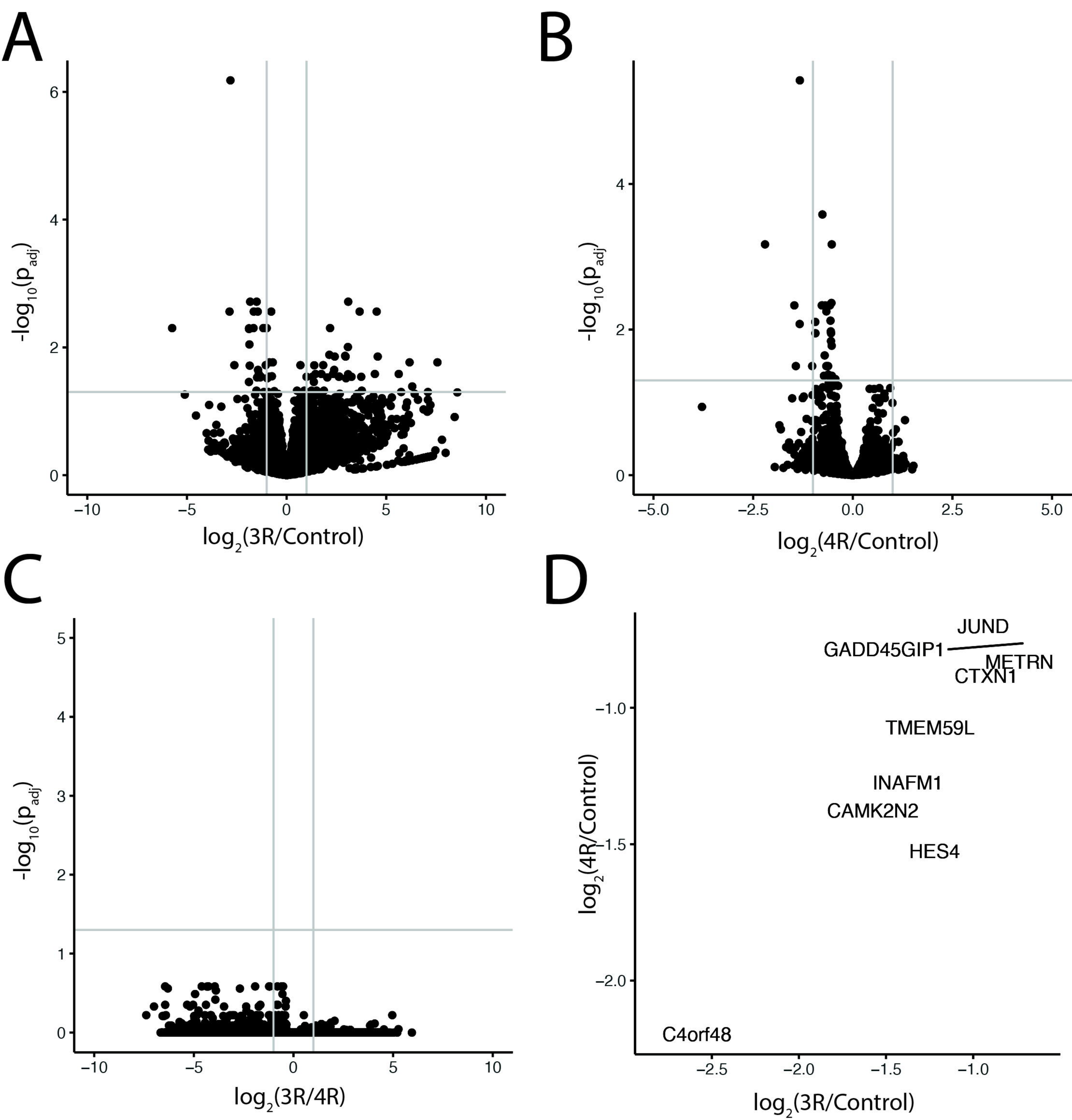
A
-log10(padj)
log2(3R/Control)
B
-log10(padj)
log2(4R/Control)
C
-log10(padj)
log2(3R/4R)
D
log2(4R/Control)
log2(3R/Control)
GADD45GIP1
JUND
METRN
CTXN1
TMEM59L
INAFM1
CAMK2N2
HES4
C4orf48

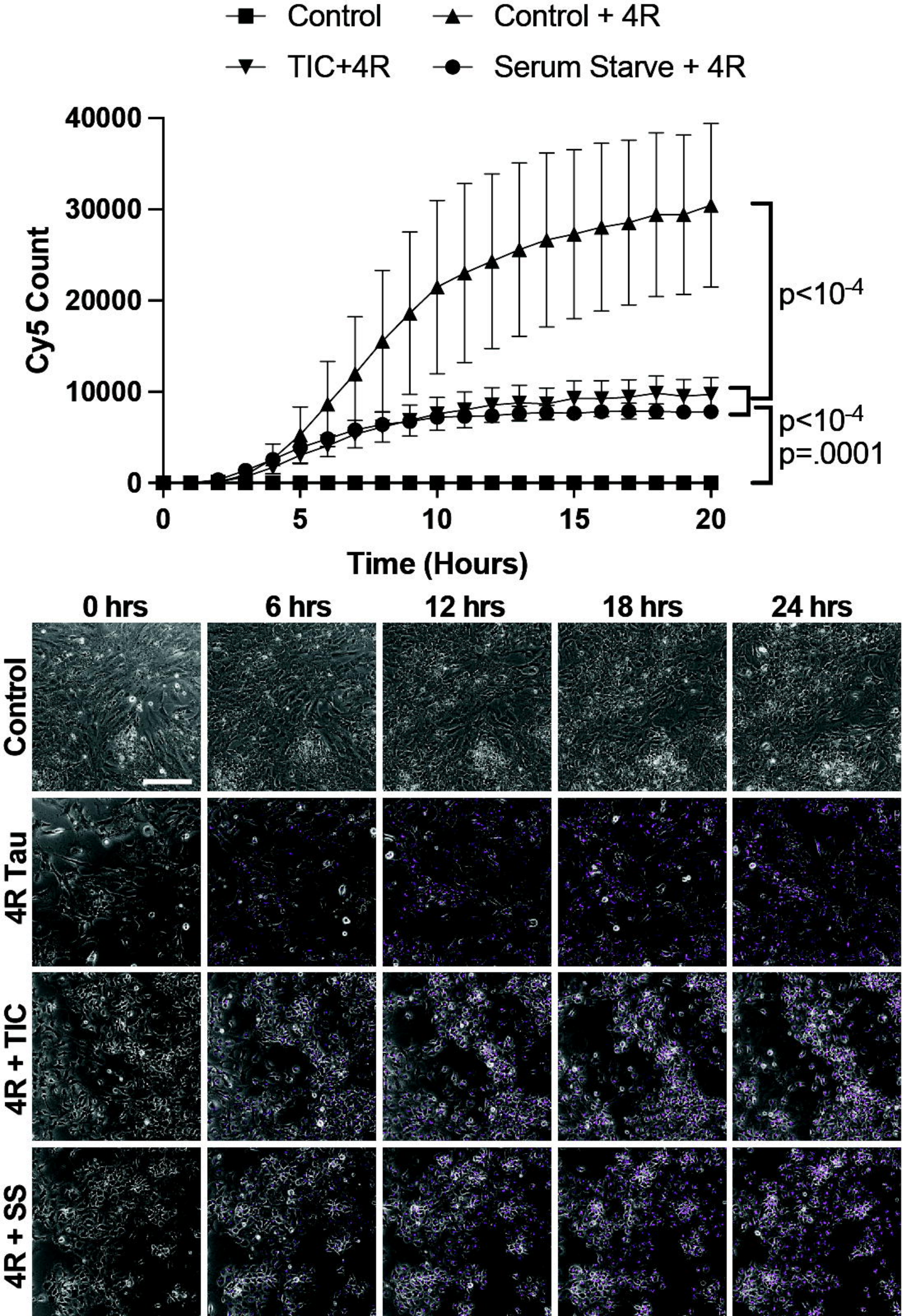
Control
Control + 4R
TIC+4R
Serum Starve + 4R
Cy5 Count
40000
30000
20000
10000
0
0
5
10
15
20
Time (Hours)
p<10-4
p<10-4
p=.0001
0 hrs
6 hrs
12 hrs
18 hrs
24 hrs
Control
4R Tau
4R + TIC
4R + SS

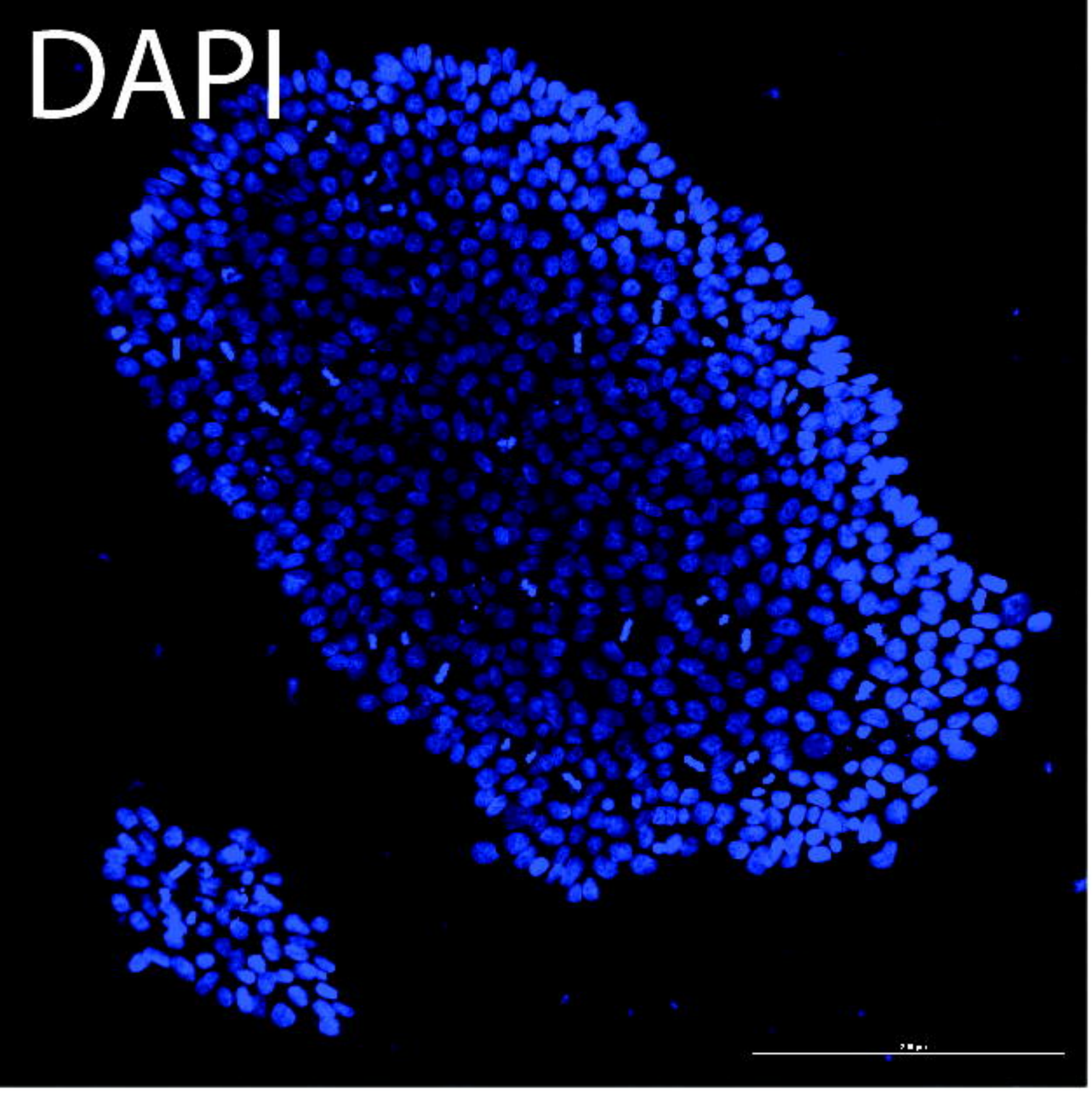
DAPI

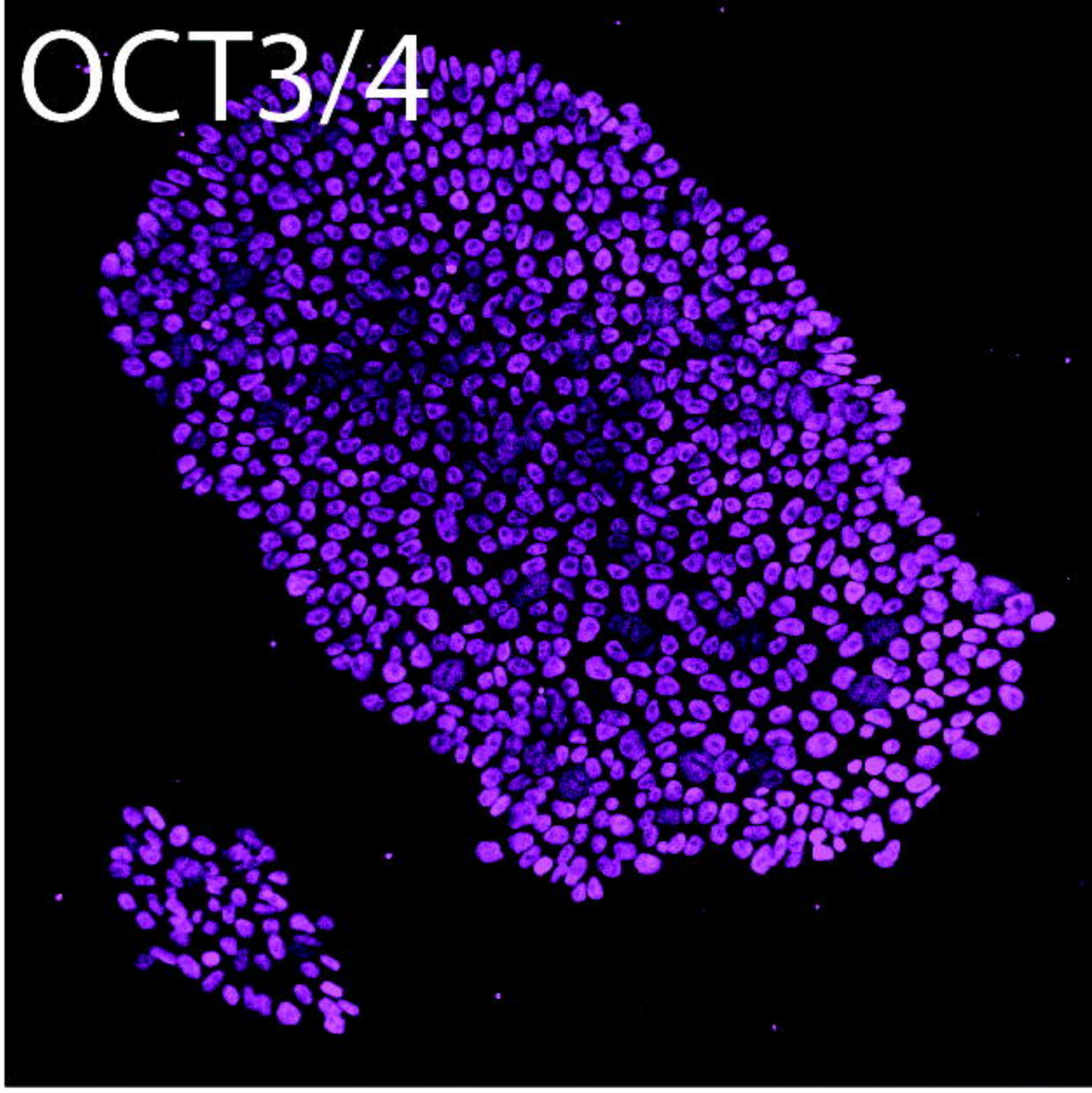
OCT3/4

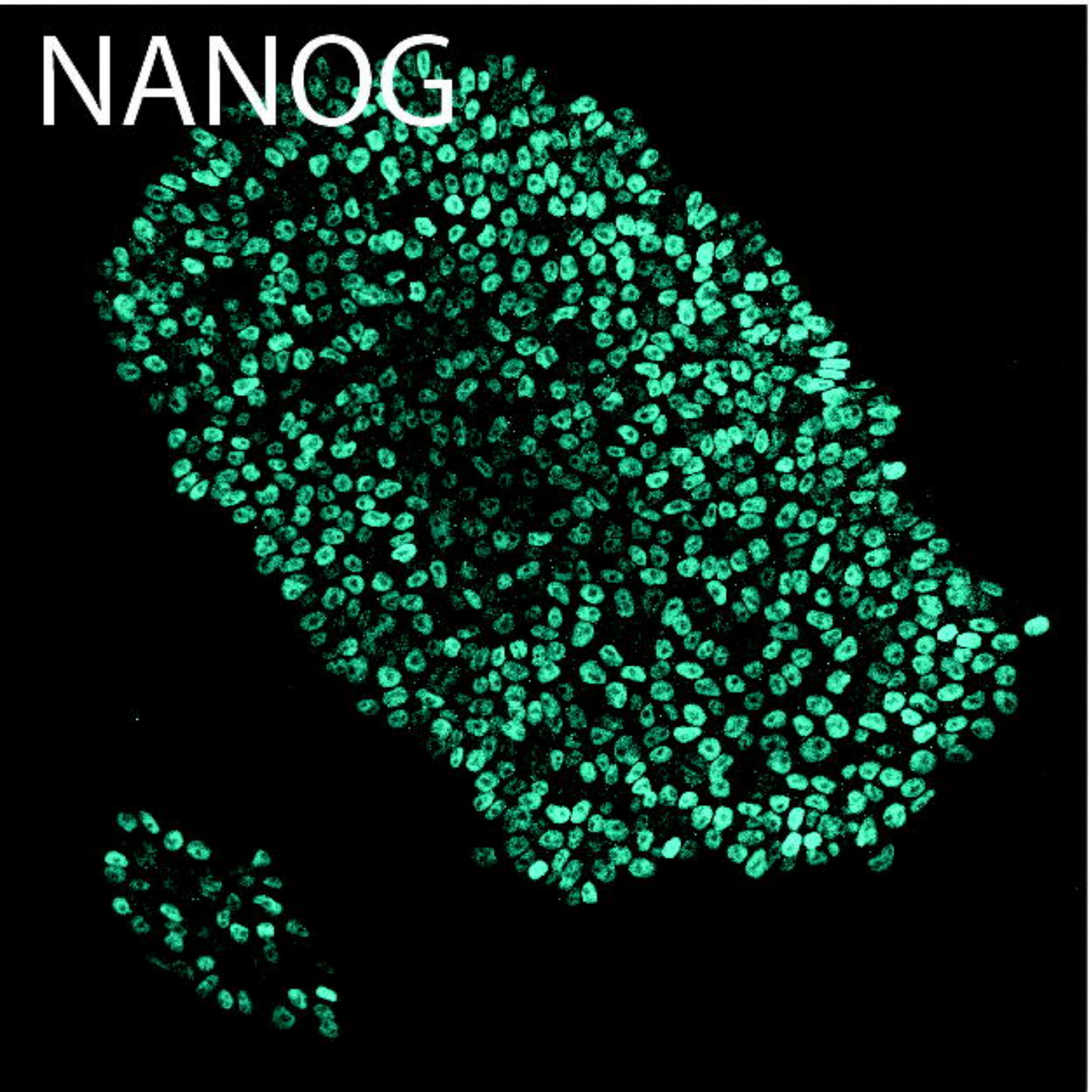
NANOG

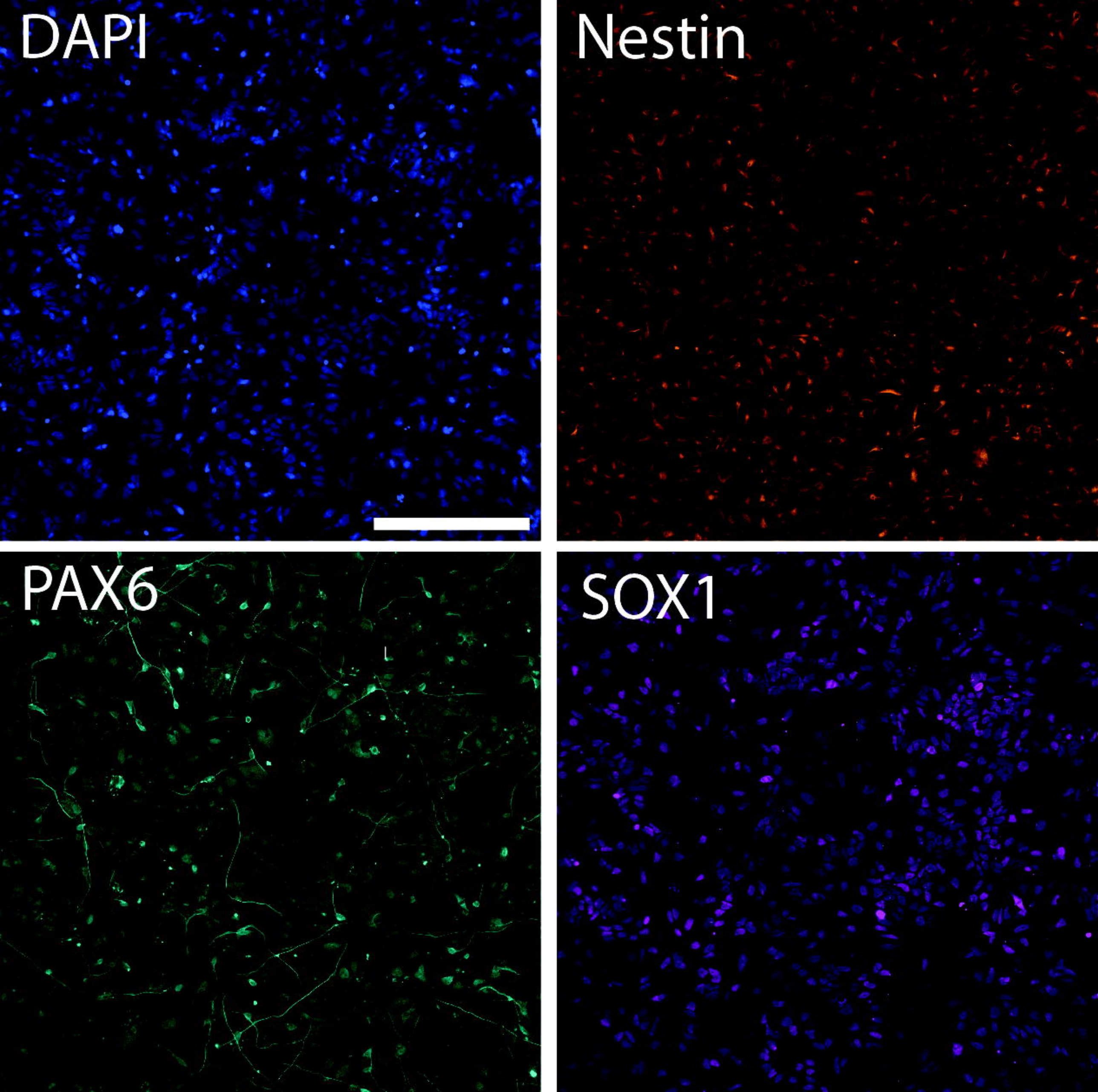
DAPI
Nestin
PAX6
SOX1

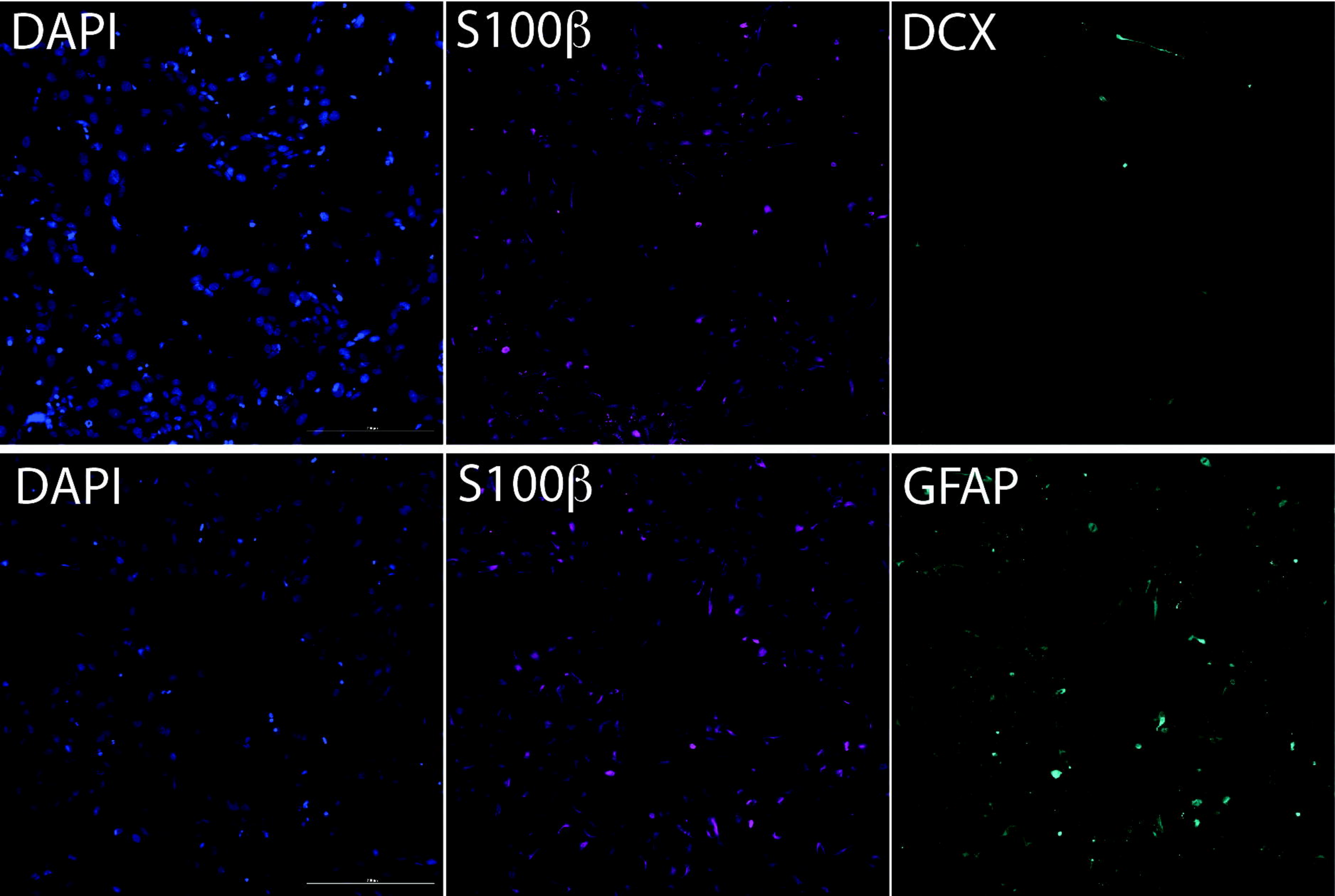
DAPI
S100β
DCX
DAPI
S100β
GFAP

H14 Endoderm

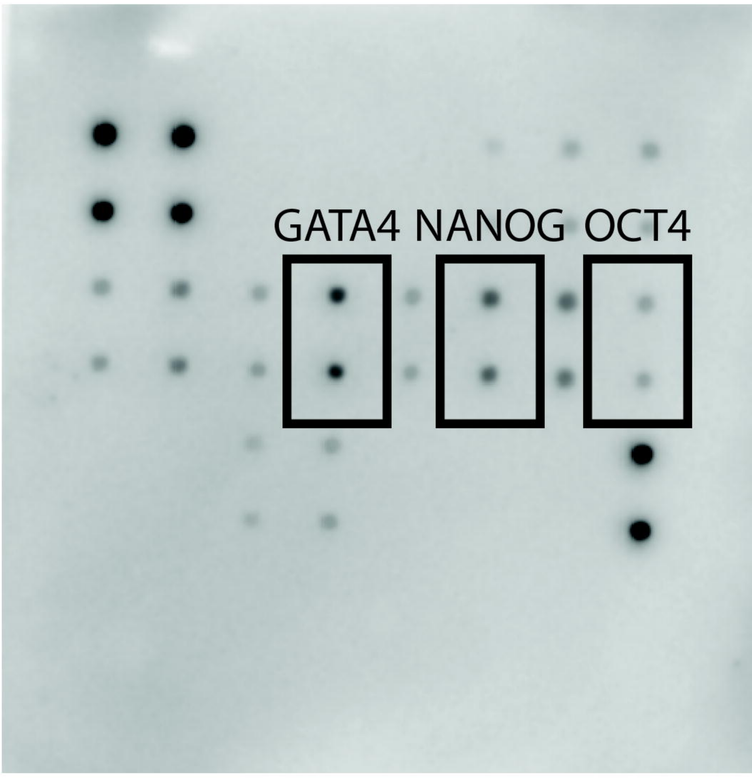

H14 Mesoderm

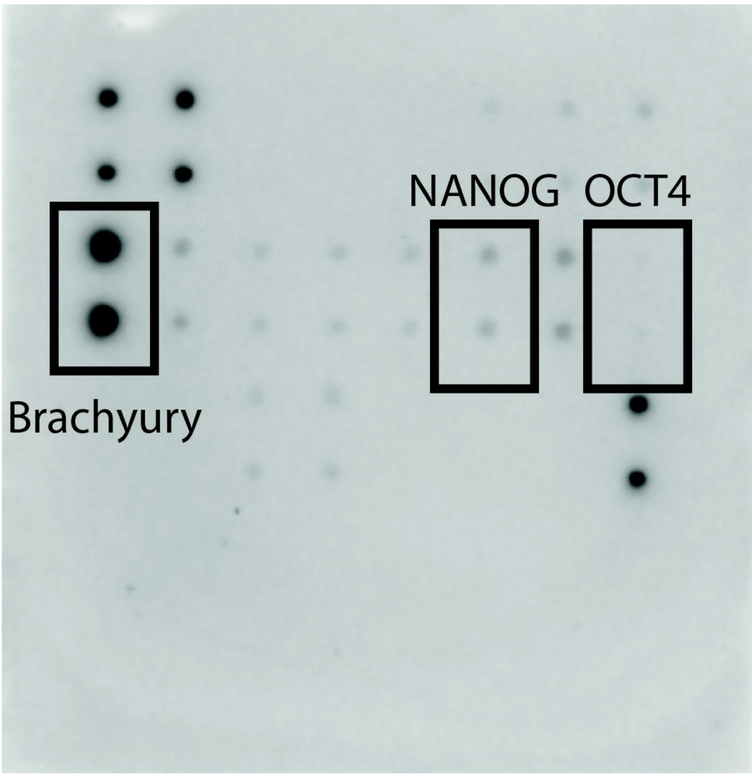

H14 Ectoderm

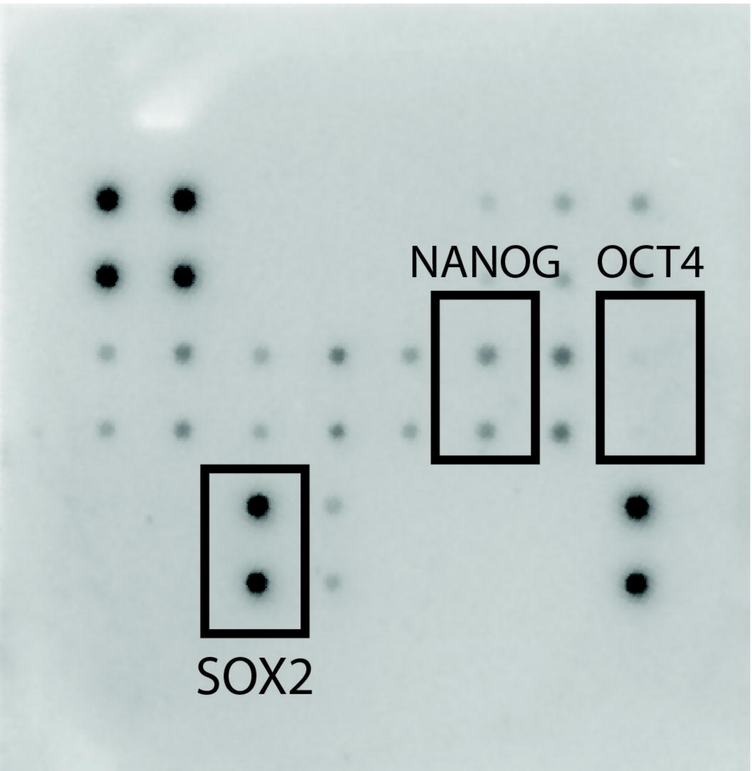

A

TauB
TauE
70kDa
60kDa

B

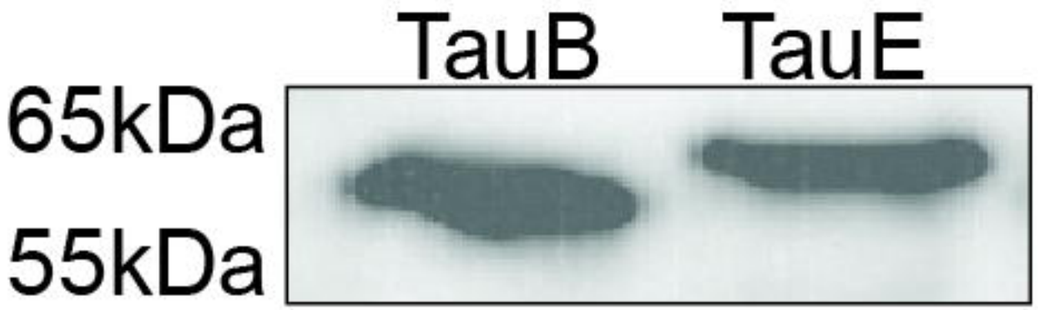
TauB
TauE
65kDa
55kDa

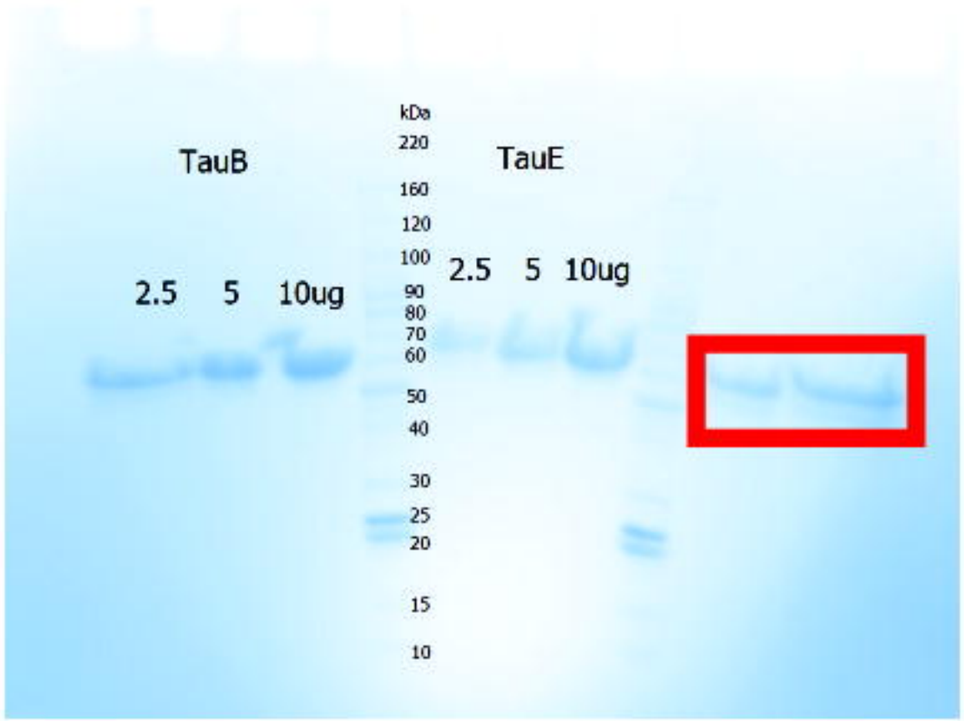
kDa
220
160
120
100
90
80
70
60
50
40
30
25
20
15
10
TauB
2.5 5 10ug
TauE
2.5 5 10ug

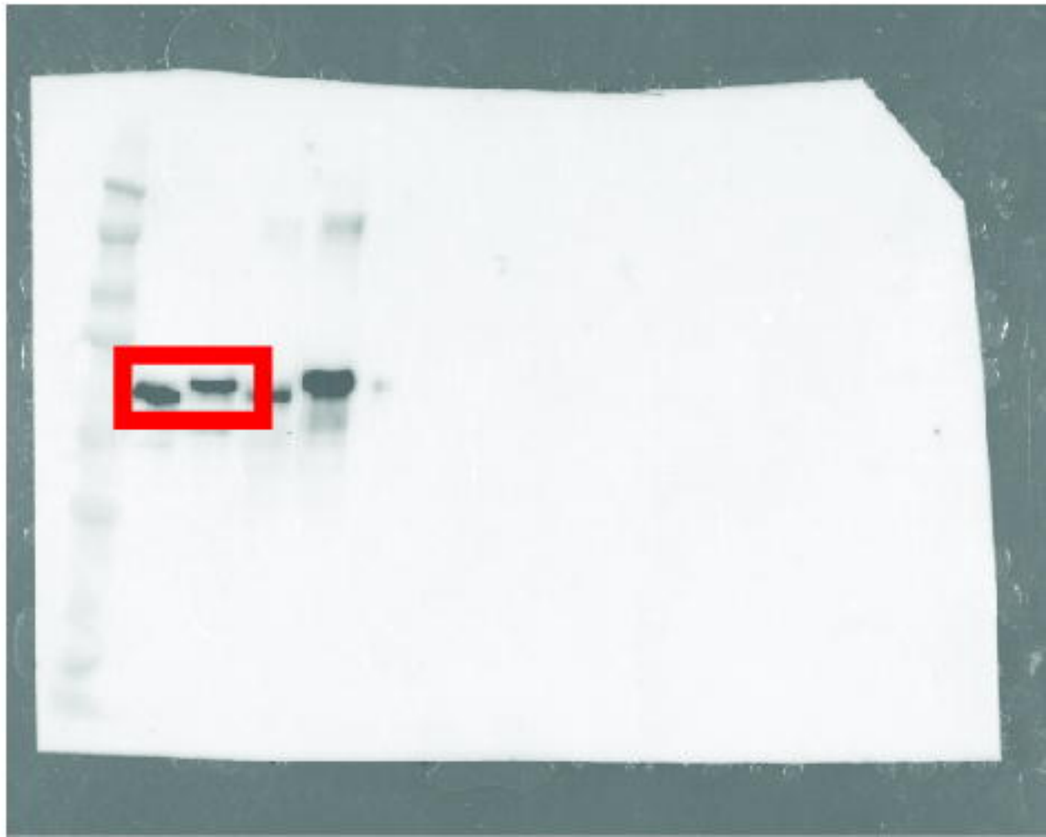

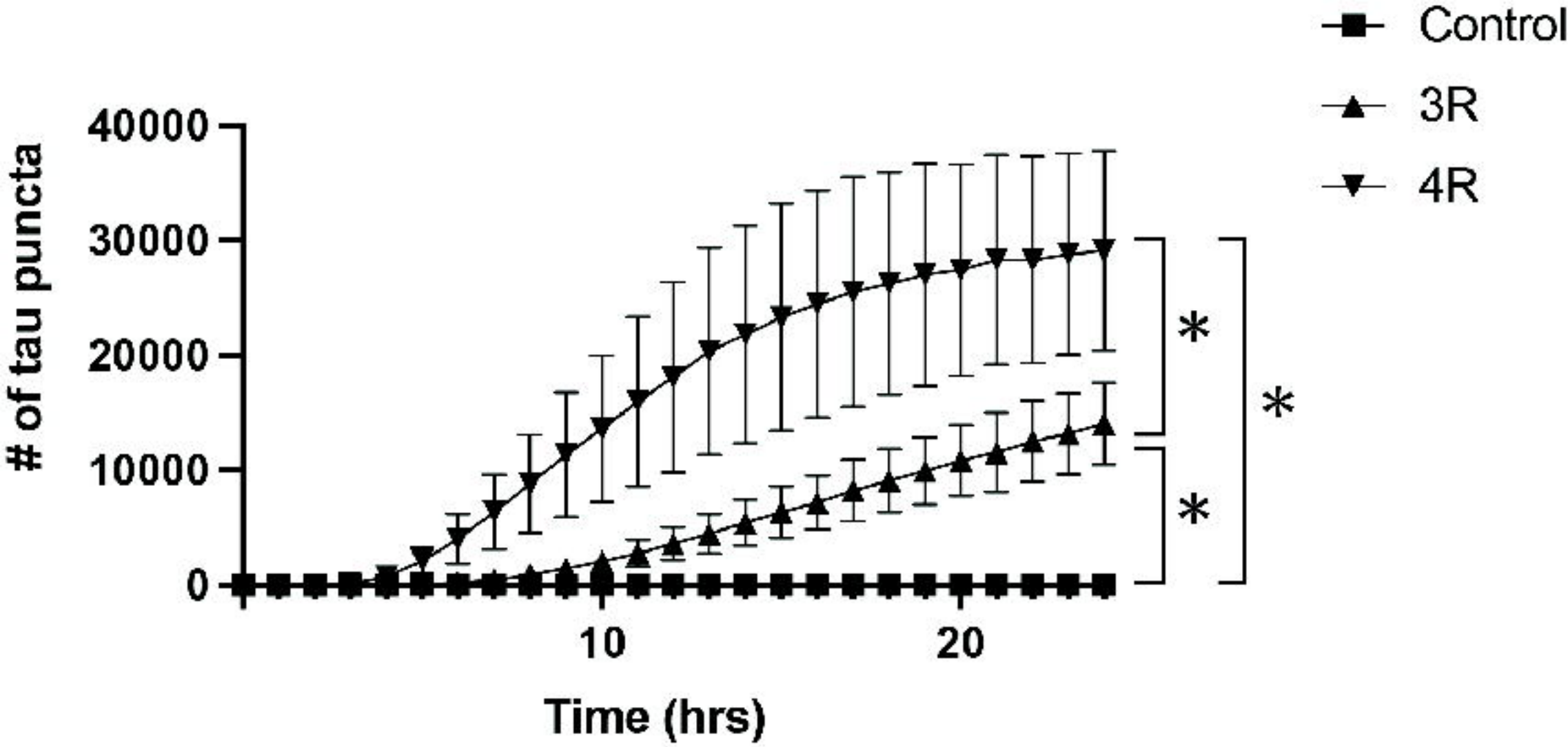
Control
3R
4R
40000
30000
20000
10000
0
# of tau puncta
10
20
Time (hrs)
*
*
*